

Multiproxy reconstruction for Kuroshio responses to Northern Hemispheric Oceanic Climate and Asian Monsoon since Marine Isotope Stage 5.1 (~88 ka)

X. Shi¹, Y. Wu¹, J. Zou¹, Y. Liu¹, S. Ge¹, M. Zhao², J. Liu¹, A. Zhu¹, X. Meng¹, Z. Yao¹ and Y. Han¹

¹Key Laboratory of Marine Sedimentology and Environmental Geology, First Institute of Oceanography, State Oceanic Administration, Qingdao 266061, China

²Key Laboratory of Marine Chemistry Theory and Technology (Ocean University of China), Ministry of Education/Qingdao Collaborative Innovation Center of Marine Science and Technology, Qingdao 266100, China

Correspondence to: Xuefa Shi (xfshi@fio.org.cn)

Abstract

The Kuroshio, a western boundary current in the ~~Northwestern~~ Western Pacific, plays a key role in regulating ocean and climate in the East Asia. The evolution of the Kuroshio and its branches has been the focus of paleoceanographic studies. In this study, we applied a multiproxy (grain size, planktonic foraminiferal species, $\delta^{18}\text{O}$, alkenone sea surface temperature (SST) and salinity) reconstruction from sediment core CSH1, which is located at the main axis of the Tsushima Warm Current, a branch of the Kuroshio, in the northern Okinawa Trough (OT). This study, ~~for the first time,~~ extended the paleoceanographic record of the Kuroshio to Marine Isotope Stage (MIS) 5.1 (~88 ka) from the far northern site in the OT. ~~The core CSH1 contains three volcanic layers, K-Ah, AT and Aso-4, which are ideal chronostratigraphic markers for precise age controls of the core.~~ Planktonic foraminiferal species identified from this core contain warm water species related to the Kuroshio and cold species related to subarctic water mass. The relative abundances of the warm water species are high during MIS 1 and MIS 5.1, while cold species are high during MIS 2. An organic biomarker proxy, alkenone SST measured from CSH1 ranges between 21–25°C with higher

values during interglacials (MIS 1, 3.3, 5.1) and interstadials, and lower values during glacials and Heinrich (H)/stadial events. Sea surface salinity (SSS) and the depth of thermocline (DOT) reconstructed based on foraminifera isotopes and faunas indicate dominant Kuroshio responses to ~~Northern Hemispheric abrupt~~ climate change event recorded in Greenland ice core and in stalagmite of East China- and Asian Monsoon (AM) since ~88 ka. The CSH1 SSS appears to be mainly controlled by the local river runoff and ~~open ocean water~~ the Kuroshio, while the DOT change seems to be closely related to the strength of Kuroshio and the latitudinal shift of subarctic frontal zone. Our records suggest that during MIS 1 and MIS 5.1 while global sea level was high, the Kuroshio was dominant; while during MIS 2, MIS 3 and MIS 4 with low sea level, stronger winter AM and more southward subarctic front played important roles in governing the hydrographic characteristics in the OT. Spectral analysis of our multiproxy hydrographic records shows a dominant precessional period at ~24 ka. Our ~~multiproxy~~ hydrographic records, such as SST, SSS and DOT, records from site near the modern Tsushima Warm Current show homogenous-accordant regional responses mainly to the global sea level ~~and, Northern Hemispheric climate, and regional mechanisms such as the~~ Kuroshio, AM and subarctic front, which are consistently invoked in the interpretations of other regional records from the OT.

1 Introduction

The meridional heat transport by ocean current plays a critical role in setting the global energy balance and regulating climate change, such as the Gulf Stream in the North Atlantic and the Kuroshio in the North Pacific. The Kuroshio carries large amount of heat, salt and moisture from the low latitude intruding into the Okinawa Trough (OT) with high current velocity, great volume transport and narrow width to far northwestern Pacific. It exerts great influence on the climate and environmental conditions of East Asia (Hsueh, 2000; Hsueh et al., 1992). In the northern OT, two branches of Kuroshio, Tsushima Warm Current (TWC) and Yellow Sea Warm Current, enter into the Sea of Japan through the shallow Tsushima Strait with a sill depth of 130 m and the Yellow Sea, respectively, while the main stream of Kuroshio continues to flow northwardly along the east coast of Japan and turn across the northwestern Pacific at ~38°N. Besides the Kuroshio, the climate of the western Pacific is also regulated by the Asian Monsoon (AM). The freshwater discharged by Yangtze and Yellow Rivers directly influences the surface water salinity and the primary productivity and therefore the organic

carbon export and burial in the adjoining continental margins. Since OT is located adjacent to the wide shelf of the East China Sea (ECS), abundant information of past climate and oceanographic changes with high resolution could be extracted from marine sediment cores from the OT because of very high sedimentation rate in the OT.

Previous studies on past climate changes using sediment cores from the OT show orbital-scale (Ijiri et al., 2005; Kao et al., 2006a; Kawahata et al., 2006; Zhou et al., 2007) and millennial and abrupt climatic responses, such as 8.2 ka, Younger Dryas, Heinrich (H) events, Dansgaard–Oeschger cycles of the Kuroshio (Chang et al., 2009; Chang et al., 2008; Ijiri et al., 2005; Li et al., 2001; Liu et al., 2001; Yu et al., 2009). However, most of these studies were limited by either shorter cores or single proxy reconstruction (Jian et al., 1998; Kao et al., 2006b; Lee et al., 2013; Ujiie and Ujiie, 1999) that covered only a small spatial scale of the OT into which the Kuroshio has intruded. In this study, we presented a multiproxy reconstruction of the Kuroshio responses from core CSH1 located at the northernmost site of the OT (Fig. 1). Our records of Kuroshio responses reconstructed here was dated back to Marine Isotope Stage (MIS) 5.1 (~88 ka), which is so far the longest record, with resolution high enough to infer the orbital to millennial scale climate and oceanographic changes in the northern OT.

2 Oceanographic background

The OT is a back-arc basin of the Ryukyu trench - arc - basin system (Lee et al., 1980). It is bounded by the Ryukyu ridge and Trench to the East and the wide shelf of the East China Sea (ECS) to the west, ~~and extends from the Ilan plain in the northern Taiwan and to the shallow sea of Kyushu in the southern Japan.~~ The entire complex is arcuate, convex toward the Pacific with a alignment of NNE—SSW from Japan to Taiwan (Lee et al., 1980). The OT is a big graben represented by the topographic depression behind the Ryukyu arc with a length of 1200 km and a width of 100–150 km. Since the middle Miocene with the opening of the OT (Sibuet et al., 1987), it has been a depositional center in the ECS and has received a huge sediment supply from nearby continents.

The modern hydrographic characteristics of surface water masses in the OT are controlled by the ~~East China Coastal Water~~ Yangtze River runoff and the Kuroshio (Lie and Cho, 2002). The ~~East China Coastal Water~~ Yangtze River carries huge amount of terrigenous materials and nutrients into the OT (Lie et al., 2003), which are responsible for the high surface productivity

in the ECS. The Kuroshio is characterized by high temperature and high salinity. After diverting from the North Equatorial Current (Sawada and Handa, 1998), it flows across the Philippine Sea and along the east Taiwan, intruding into the OT and flows northwardly along the trough. In the northern OT and the southern Kyushu, the main axis of the Kuroshio turns eastward, crosses the Ryukyu Arc through the Tokara Strait and then continues to flow north eastwardly into the northwestern Pacific Ocean at $\sim 38^{\circ}\text{N}$. Another branch of the Kuroshio, called TWC, flows into the Sea of Japan through the Tsushima Strait. Because of the strong intrusion of the Kuroshio, the hydrographies are characterized by high temperature and salinity, deep depth of thermocline (DOT) in the OT (Jian et al., 2000a). In contrast, the hydrographies are characterized by lower temperature and salinity, shallow DOT in the adjacent ECS shelves.

In our study area, the instrumental hydrographic records of the past century (1874–2002) show high temperature and low salinity in the upper water column ($<100\text{ m}$) in boreal summer (Fig. 2). Below 100 m, the seasonal ranges of water temperature and salinity show only small changes. Previous investigations showed that the Changjiang river plume could move eastward over 400 km offshore across the wide shelf of the northern East China Sea when southerly winds prevail (Lie et al., 2003). ~~Modeling results indicate that a plume of lower salinity water entered into the northern OT, which in turn flowed into the Sea of Japan during the mega flood of Yangtze River in 1998 (Watanabe, 2007).~~

3 Materials and methods

The core CSH1 ($31^{\circ}13.7'\text{N}$, $128^{\circ}43.4'\text{E}$, water depth 703 m) was taken from the northern OT with a length of 17.3 m using a piston corer during the XiangYangHong Cruise in 1998. The sediments of the core mainly consist of black-grey and grey silt or clayey silt with and shell fragments and foraminifera occurring throughout the core (Ge et al., 2007). Initial core descriptions for CSH1 indicated that the core is continuous without interruptions by any visible turbidites but contains three volcanic ash layers (Ge et al., 2007; Wu et al., 2004). In this study, we performed high-resolution sampling by 4 cm intervals that resulted in a total of 434 samples for this analysis. Based on our AMS ^{14}C dating and $\delta^{18}\text{O}$ stratigraphy of planktonic foraminifera (Table 1), the bottom age of CSH1 is $\sim 88\text{ ka}$, equivalent to MIS 5.1 (Fig. 3).

3.1 Grain size analysis

The sediment grain size was measured by Malvern MS-2000 laser diffraction in the Key Laboratory of Marine Sedimentology and Environment Geology in the First Institute of Oceanography, SOA. The equipment has a dynamic range of 0.02–2000 μm with a resolution of 0.01 ϕ . After removing the organic matter (10% H_2O_2) and carbonate (1 M HCl) from the sediment samples, the residual samples were standing for 12 h to make it fully precipitated. The residual were then measured for grain size analysis after adding into sodium hexametaphosphate.

3.2 Planktonic foraminiferal fauna analysis

The samples for planktonic foraminiferal fauna analysis was firstly dried in the oven at 50°C and weighted and then placed in water for 72 h. The samples were washed through a 63 μm sieve to remove the fine fraction and the identification of planktonic foraminiferal fauna specimens was done based on census counting of at least 300 specimens >154 μm . All 26 species of planktonic foraminifera were identified and the relative abundances of each planktonic foraminiferal species were calculated based on the classification scheme (Table 2).

3.3 Analysis for $\delta^{18}\text{O}$, $\delta^{13}\text{C}$ and AMS ^{14}C

Stable oxygen and carbon isotopes ($\delta^{18}\text{O}$ and $\delta^{13}\text{C}$ vs Pee Dee Belemnite, respectively) of 199 downcore samples were measured using ~30 specimens of planktonic foraminifera *Globigerinoides ruber* using IsoPrime stable isotope mass spectrometer in the Bremen University. The analysis error for $\delta^{18}\text{O}$ and $\delta^{13}\text{C}$ is < 0.06‰ and 0.03‰, respectively.

Accelerator Mass Spectrometer (AMS) ^{14}C ages were measured based on analysis of ~500 specimens of *Neogloboquadrina dutertrei* (>150 μm) at 12 stratigraphic horizons using the AMS in the Leibniz-Laboratory for Radiometric Dating and Isotope Research (Table 1).

3.4 Alkenone sea surface temperature (SST) analysis

Dried and homogenized sediment samples were extracted three times using a mixture of dichloromethane and methanol (97:3). The unsaturated alkenones were isolated from sediment extracts dried using rotary evaporation and saponified with a 0.5 M solution of KOH in MeOH. After drying under nitrogen gas, the extracts were separated into four fractions using column chromatography. $\text{N-C}_{36}\text{H}_{74}$ was added as an internal standard to alkenone.

Unsaturated alkenones were analyzed using a HP6890 Gas chromatography with on-column injection, an electronic pressure control system, and a flame ionization detector. The experimental procedures of using a GC column and setting up an oven temperature and carrier pressure programs were reported by Xing et al. (2008). The long chain unsaturated alkenones were measured in the China Ocean University. SST was calculated using the following equations (Muller et al., 1998):

$$U_{37}^k = C_{37:2Me} / (C_{37:2Me} + C_{37:3Me}) \quad (1)$$

$$SST (^{\circ}C) = (U_{37}^k - 0.044) / 0.033 \quad (2)$$

The analytical error for U_{37}^k is 0.006 which translates into an error of 0.2 $^{\circ}$ C in estimating SST.

3.5 Salinity

The planktonic foraminifera $\delta^{18}O$ ($\delta^{18}O_{pf}$) is controlled by seawater $\delta^{18}O$ ($\delta^{18}O_{sw}$) and local SST. In the northern OT, higher contents of unsaturated alkenones observed in the upper water column of ~20 m and the estimated temperature is consistent with the modern observation based on the sediment trap samples (Nakanishi et al., 2012). Coccolithophore fluxes are high throughout the year, except for summer season in the ECS (Tanaka, 2003). Therefore, alkenone - derived SST could be used to obtain annual mean SSS estimates in the northern OT. For *G. ruber*, Mulitza et al. (2004) established the following correlation between temperature and $\delta^{18}O$:

$$T = 14.32 - 4.28 \times (\delta^{18}O_{pf} - \delta^{18}O_{sw}) + 0.07(\delta^{18}O_{pf} - \delta^{18}O_{sw})^2 \quad (3)$$

where $\delta^{18}O_{sw}$ is related to local SST and evaporation and precipitation. In the areas influenced by the Kuroshio, there is a relationship between salinity and $\delta^{18}O_{sw}$ (Oba, 1988) as follows:

$$\delta^{18}O_{sw} = 0.203 \times SSS - 6.76 \quad (4)$$

In 2006, a total of 317 seawater samples collected from the Yellow Sea and ECS were analyzed for salinity and $\delta^{18}O_{sw}$ that resulted in the following correlation (Du et al., 2012):

$$\delta^{18}O_{sw} = 0.29 \times SSS - 9.85 \quad (5)$$

The $\delta^{18}O$ values in the water from Yangtze and Yellow Rivers range ~ -8.8 to -7.1‰ (Zhang et al., 1990), which is consistent with the intercepts in the equations (4) and (5) and therefore both equations (4) and (5) are considered as a mixing between local runoff and seawater in the

marginal seas. After removing the effect of global ice volume on $\delta^{18}\text{O}_{\text{sw}}$ (Bintanja et al., 2005), the salinity in core CSH1 was calculated. The conversion relationship for $\delta^{18}\text{O}$ of calcite relative to VPDB is as follows (Coplen, 2007):

$$\delta^{18}\text{O}_{\text{V-SMOW}} = 1.03092 \times \delta^{18}\text{O}_{\text{PDB}} + 30.917\text{‰} \quad (6)$$

In order to minimize the errors of $\delta^{18}\text{O}$ subtraction from two isotope records, the raw data were smoothed using five-point running average procedure. The salinity calculated based on both equations (4) and (5) shows a similar trend. Here, we use equation (5) to calculate the CSH1 SSS record.

3.6 Age model

The age model for CSH1 was built by AMS ^{14}C and planktonic foraminifera $\delta^{18}\text{O}$ SPECMAP age controls. In the upper 1002 cm, the age control points were determined by AMS ^{14}C , while below 1002 cm, the age model was constructed by SPECMAP chronology (Table 2). A preliminary age model of the last 40 ka for core CSH1 was built using 4 AMS ^{14}C data based on mixing planktonic foraminiferal specimens (Chen et al., 2006). In this study, we constructed a more precise age model by picking up single species *N. dutertrei* for AMS ^{14}C dating from 12 samples, of which 5 AMS ^{14}C dating below the core depth 1002 cm are older than 40 ka and are unused. All other AMS ^{14}C dates show no reversals (Table 2). Combined with previously reported 4 AMS ^{14}C dates, all 11 AMS ^{14}C ages were calibrated into the calendar year by a correction for an average surface ocean carbon reservoir of 400 years (Calib 6.1) (Reimer et al., 2009). Considering that the calibrated calendar age (12.384-12.491 ka) at 178 cm conflict slightly with the age at 158 cm (12.220-12.392 ka), the age at 178 cm is not adopted here. In final, a total of 10 AMS ^{14}C ages were used as age control points for the upper 1002 cm in CSH1.

The $\delta^{18}\text{O}$ curve of *G. ruber* shows good correlation with SPECMAP (Martinson et al., 1987) (Fig. 3), which allows us to identify MIS 1-5.1 (Table 1). The existence of three ash layers provides independent age controls. The sediment grain size and susceptibility are increased at the ash layers (Ge et al., 2007). According to the heavy mineral composition, morphology and refractive index of volcanic glass, the first two ash layers are considered as K-Ah (6.1-7.5 ka) and AT (30-35 ka) (Machida, 1999), which are widely distributed in the Sea of Japan and the OT. The bottom ages of the two ash layers are consistent with previous results - 7.54 ka (108 cm) and 30.67 ka (796 cm), respectively. The third ash layer is recognized as Aso-4 (MIS

5.1/5.2) (Machida, 1999). However, our isotope age model indicates that the bottom of the third ash layer is ~79.44 ka (1616 cm), which is slightly younger than the absolute dating for Aso-4 (84-89 ka) (Machida, 1999). The age difference might result from the internal discrepancy between K-Ar dating method and SPECMAP chronology, and not affect our interpretation on the records.

Our combined AMS ^{14}C , SPECMAP $\delta^{18}\text{O}$, and volcanic ash layer chronology generates an estimated bottom age of ~87.4 ka for CSH1 (Fig. 4) with an averaged sampling resolution of ~200 years. The calculated linear sedimentation rate (LSR) varies from $>40 \text{ cm ka}^{-1}$ during MIS 2 and MIS 3 to $<10 \text{ cm ka}^{-1}$ in the last deglaciation (7.5-12.3 ka) and MIS 4 (55.5-64.1 ka).

4 Results

4.1 Grain size analysis

The grain size analysis reveals that the sediment mainly consists of silt and clayey silt, which varies between 36-81 % (Fig. 5). In ash layers, the sand content increases significantly, while clay and silt contents decrease. The frequency distribution for sediment grain size shows a single peak in normal sediment layers, while a bimodal peak is shown in the ash layers. Except for the volcanic ash layers, the mean grain size increased during MIS 5.1 and since the last deglacial period (Fig. 5).

4.2 Planktonic foraminiferal assemblages

A total of 27 planktonic foraminiferal species were identified and counted and of which the average abundances of 11 species are $>1\%$. These 11 species constitutes 86% of the planktonic foraminiferal assemblage. From high to low average abundances, they are *Globigerina bulloides*, *N. dutertrei*, *G. ruber*, *Neogloboquadrina pachyderma* (dex.), *Globigerinita glutinata*, *Globorotalia inflata*, *Globigerina quinqueloba*, *Pulleniatina obliquiloculata*, *Globigerinoides sacculifer*, *Globigerina falconensis*, and *Globigerinoides tenellus* (Table 2).

The planktonic foraminiferal assemblage in CSH1 consists of many cold water species. For example, *N. dutertrei* mainly lives in the thermocline below the mixed layer and is a dominant

1 species in core CSH1 with an average value of 21.6%. The highest abundance of *N. dutertrei*
2 occurred during the LGM (26.6%) and MIS 5.1 (26.2%), while lower abundance appeared
3 during MIS 1 (15%) (Fig. 6; Table 2). In the tropical and subtropical Atlantic, higher
4 abundances of *N. dutertrei* are mainly related to upwelling (Pflaumann et al., 1996) and are
5 indicative of the upwelling zones in the South China Sea (SCS) (Pflaumann and Jian, 1999).
6 *N. pachyderma* (dextral), is a cold water species dominant in the Arctic and subarctic
7 oceans (Hemleben et al., 1989). In core CSH1, the abundances of *N. pachyderma* (dextral)
8 were 2.5% and 6.7% during MIS 1 and MIS 5.1, respectively; while during MIS 2, MIS 3 and
9 MIS 4, its abundances were relatively high with 15.3%, 11.3% and 12.7%, respectively.
10 Except during MIS 5.1, abundances of *N. pachyderma* (dextral) were well paralleled with *N.*
11 *dutertrei*. The abundance of *G. quinqueloba* were higher during MIS 2 and MIS 4 than during
12 MIS 1 and MIS 5.1, with an average value of 2.3% and also show a similar trend with *N.*
13 *pachyderma* (dextral) (Fig. 6). *G. inflata* is a “gyre margin” species in the world
14 ocean (Hemleben et al., 1989), and the high abundances of *G. inflata* occur at the convergence
15 zone between the Kuroshio and subpolar water mass in the western Pacific (Thompson, 1981).
16 In core CSH1, the abundances of *G. inflata* were lower during MIS 1 (3.1%) and MIS 2
17 (3.7%) than those in MIS 3 (5.5%), MIS 4 (6.6%) and MIS 5.1 (6.5%) (Fig. 6).

18 Among warm water species in CSH1, *G. ruber* is the most dominant and shows high
19 abundances during interglacials and low during glacials (Fig. 6). The *G. ruber* abundances
20 gradually increased since 16 ka and reached a maximum in the mid-Holocene. The *G. ruber*
21 abundances decreased during H events, but showed relatively high during the LGM. Another
22 warm water species, *G. glutinata* shows similar abundance pattern with *G. ruber*. The average
23 abundances of warm water species *P. obliquiloculata* and *G. sacculifer* are <2%, but show
24 similar patterns with *G. ruber*. However, the abundances of *P. obliquiloculata* were
25 characterized by maxima during MIS 5.1, which were not seen in other warm water species
26 (Fig. 6). ~~The maxima in MIS 5.1 may imply a change of Kuroshio strength, as suggested by~~
27 ~~previous micropaleontological studies (Li et al., 1997).~~

28 The presence of *G. bulloides* and *Globorotalia truncatulinoides* in CSH1 indicate changes in
29 upwelling. *G. bulloides* is dominant with an averaged abundance of 22.4%, second only to *N.*
30 *dutertrei*. Interestingly, the abundances of *G. bulloides* reached maxima during MIS 3 (27.8%)
31 and minima during MIS 1, MIS 2, MIS 4 and MIS 5.1. (Fig. 6) The average abundances of *G.*
32 *truncatulinoides* are relatively low in CSH1, but show interestingly morphotype changes in

coiling directions. The sinistral morphotype was dominated during 51-88 ka, while the dextral was more dominated after 51 ka (Fig.9). Since the Holocene, the abundances of dextral were decreased and were rarely found during 4-8 ka, consistent with the previous study from the SCS (Jian et al., 2000b).

In order to reveal the correlation between the abundances of planktonic foraminiferal species, a Q-mode VARIMAX factor analysis was used based on the abundance data of planktonic foraminiferal species from core CSH1, and four factors that explain 96% of the total variance were extracted (Table 2). Factor 1 explains 45% of the total variance, and is composed solely by the upwelling species, *G. bulloides*. Factor 2 explains 23% of the total variance, and is mainly composed by numerous warm water species - *G. ruber*, *G. conglobatus*, *G. rubescens*, *G. tenellus*, *G. glutinata*, *G. sacculifer*, *P. obliquiloculata*. Factor 3 explains 16% of the total variance, and consists of cold water water species - *G. quinqueloba*, *N. pachyderma*. Factor 4 explains 12% of the total variance, mainly composed by species indicative of shallow-DOT or convergence zone between water masses - *N. dutertrei* and *G. inflata*.

4.3 Stable carbon and oxygen isotopes of planktonic foraminifera

The values of $\delta^{18}\text{O}$ from *G. ruber* vary between -2.54‰ and -0.11‰, and were heavier during MIS 2, MIS 3 and MIS 4 than those during MIS 1 and MIS 5.1 (Table 2 Fig. 7). In contrast to MIS 1, the values of $\delta^{18}\text{O}_{\text{ruber}}$ during MIS 1 were much heavier than those in MIS 5.1 (Fig. 7 Table 2), although SST values were close during both intervals. In spite of its high frequency variation, $\delta^{18}\text{O}_{\text{ruber}}$ with 5-point running average in core CSH1 matches well with the SPECMAP (Martinson et al., 1987), indicating the first order pattern of $\delta^{18}\text{O}_{\text{ruber}}$ was driven by global ice volume. The $\delta^{18}\text{O}_{\text{ruber}}$ gradually decreased since 18 ka and reached minima during early Holocene (Fig. 7). Such trends were also observed in previous results from cores MD982195 (Ijiri et al., 2005) and core A7 (Sun et al., 2005) and KY07 (Kubota et al., 2010) in the northern and middle OT, ODP184-1144 (Buhring, 2001) and MD972142 (Chen et al., 2003) in the SCS. Fig. 7 shows that the values of $\delta^{18}\text{O}_{\text{ruber}}$ in core CSH1 are higher than those recorded in the SCS. In spite of its high frequency variation, $\delta^{18}\text{O}_{\text{ruber}}$ with 5-point running average in core CSH1 matches well with the SPECMAP (Martinson et al., 1987), indicating the first order pattern of $\delta^{18}\text{O}_{\text{ruber}}$ was driven by global ice volume.

The value of $\delta^{13}\text{C}_{\text{ruber}}$ ranges between -0.61‰-1.45‰ and -1.45‰-0.61‰ with the lowest values in H2 (24 ka) and gradually became heavier since 24 ka then (Fig. 7). The ^{13}C enrichment is

also recorded in Site 184 (Buhring, 2001), MD972142 (Chen et al., 2003) and MD982195 (Ijiri et al., 2005). However, during MIS 5.1, $\delta^{13}\text{C}_{\text{ruber}}$ showed reverse trend in contrast to site ODP184 (Buhring, 2001) and core MD972142 (Chen et al., 2003). $\delta^{13}\text{C}$ value in planktonic foraminiferal shell is controlled by many factors, including the $\delta^{13}\text{C}$ of the local seawater, vital effects, the habitat fauna species and post-depositional dissolution (Mulitza et al., 1999). ~~Gradually heavier $\delta^{13}\text{C}$ values of *G. ruber* in CSH1 are most likely caused by the increased fixation of light carbon (^{12}C) by the expansion of continental vegetation related to the climate warming, which results in the enrichment of heavy carbon (^{13}C) in the ocean.~~ The difference between $\delta^{13}\text{C}$ curves from CSH1, Site ODP184 (Buhring, 2001), and MD972142 (Chen et al., 2003) suggests different surface ocean hydrology in the OT and SCS during MIS 5.1. During 6 - 20 ka, $\delta^{13}\text{C}_{\text{ruber}}$ values in core DGKS9603 from the middle Okinawa Trough showed lighter values, which was interpreted as reflecting to an invasion of oligotrophic tropical Pacific water (Li et al., 2002) but not observed here in CSH1. This indicates a more complicated spatial pattern of $\delta^{13}\text{C}$ in the sea water in the OT which is far beyond our current understanding.

4.4 Alkenone SST

In core CSH1, alkenone SST varies from 21 to 25°C with an average of 23°C. The average SST during MIS 1 (24.5°C) and MIS 5.1 (24.4°C) were more or less similar and these values are much higher than MIS 2 (21.8°C), MIS 3 (23.1°C) and MIS 4 (22°C) (Table 3). The average SST since 8 ka was close to the annual mean SST from instrumental observations near the site (~24.87°C) (Table 3), indicating that the alkenone SST mainly reflects annual mean temperature, ~~while Mg/Ca SST may be biased toward summer SST (Kubota et al., 2010; Sun et al., 2005).~~ The CSH1 SST during MIS 2 and MIS 4 were similar and were lower than modern SST by 2.5°C. During the LGM, the alkenone SST varied from 21 to 22°C, with an average of 21.5°C, which was lower than modern SST by 3.4°C. Since 17 ka, the CSH1 alkenone SST values increased rapidly from 21 to 25°C. Comparing to other SST records in cores ~~A7~~, DGKS9604 and MD982195 from the OT, the CSH1 SST record shows a similar pattern but is slightly higher than MD982195 (Ijiri et al., 2005) and lower than DGKS9604 (Yu et al., 2009) (Fig. 8).

~~Considering that $\delta^{18}\text{O}_{\text{ruber}}$ in core CSH1 is controlled mainly by SST and SSS, we found that the SST difference between MIS 1 and MIS 5.1 is 0.3°C, which is translated into only 0.066‰ as a temperature effect in driving $\delta^{18}\text{O}_{\text{ruber}}$ changes. However, the $\delta^{18}\text{O}_{\text{ruber}}$~~

~~difference between MIS 1 and MIS 5.1 is 0.74‰, which is not possibly affected by temperature change. Therefore this observation suggests that the much heavier $\delta^{18}\text{O}_{\text{ruber}}$ in MIS 5.1 and whole CSH1 $\delta^{18}\text{O}_{\text{ruber}}$ record must be dominated by other factors, such as local SSS and regional precipitation versus evaporation.~~

4.5 Sea surface salinity (SSS)

Our SSS estimate for core CSH1 shows large fluctuations (Fig. 8). During MIS 1 and MIS 2, the SSS was similar (34.8 psu and 34.8 psu, respectively) (Table 3), consistent with the modern annual mean SSS (34.7 psu) near this site. The SSS values were much higher in MIS 3 (35.8 psu), MIS 4 (35.2 psu) and MIS 5.1 (36.4 psu) with maxima occurred during MIS 5.1 and mid-MIS 3 (Fig. 8, Table 3). During cold periods, such as LGM, H events/stadials, the SSS values increased. These high SSS values suggest less precipitation and/or river runoff relative to evaporation than today in the northern OT.

4.6 Depth of Thermocline (DOT)

Our DOT estimate using the planktonic foraminiferal transfer function (Andreasen and Ravelo, 1997) for CSH1, which is based on the spatial distribution of 189 core top planktonic foraminifera in the tropical Pacific. The transfer function has a standard error of 22 m and additional 5 m of error due to insufficient counts in the core top database. The result shows the changes of DOT from >160 m during MIS 1, and vary ~~from-between~~ 139 m ~~and to~~ 141 m ~~from during~~ MIS 2 to MIS 5.1 (Fig. 9). DOT in core CSH1 was rapidly increased since 15 ka but abruptly decreased during the LGM, H events/stadials, consistent with what has been observed from the middle OT (Xiang et al., 2007). Our DOT estimate is also consistent with the implications made from the changes of planktonic foraminiferal assemblages (Ravelo and Fairbanks, 1992; Ravelo et al., 1990; Thunell et al., 1983) (Fig. 9). Planktonic foraminiferal species *G. ruber*, *G. sacculifer*, *G. glutinata* are shallow water species and their abundances are increased with more deepened DOT (Fig. 9d). *N. dutertrei* and *N. pachyderma* live below the thermocline and when the DOT becomes shallower, the abundances of these deep dweller species are increased (Ravelo and Fairbanks, 1992; Ravelo et al., 1990) (Fig. 9e). ~~More interestingly, the abundances of *G. truncatulinoides* (sin.) relative to *G. truncatulinoides* (dex.) appear to reflect much deeper DOTs (Fig. 9a; b).~~ Overall, the CSH1 DOT estimates show rapid decreases during most of the cooling episodes since 88 ka, which indicate lowering of

surface water heat content by a southward movement of cold subarctic water mass, weakening of the Kuroshio, or stronger winter AM.

5 Discussions

5.1 Multiproxy hydrographic reconstructions

~~Our multiproxy reconstruction for Kuroshio responses indicates noticeable linkages to regional and global forcing.~~ The most noticeable hydrographic changes are revealed by the faunal analysis. Our faunal Factor 1, which represents the most dominant species *G. bulloides* in CSH1 (Figs. 6 and 10), serves as a proxy for local upwelling and may also indicate the changes in productivity (Anderson and Prell, 1993; Emeis et al., 1995; Peeters et al., 2002). In surface sediments in the northern OT, the abundances of *G. bulloides* are high in the ECS shelves and mainly related to lower SSS and high nutrient water with an average of 12% (Xu and Oda, 1999). In the marginal seas of northwestern Pacific, higher abundances of *G. bulloides* are mainly associated with upwelling (Ijiri et al., 2005; Xiang et al., 2007). High Factor 1 scores and *G. bulloides* abundances during late MIS 3 (Figs. 5 and 9) may link to ~~strong upwelling a sea level fall at that time,~~ with an increased nutrient supply ~~from nearby rivers~~ that triggered high productivity.

The faunal Factor 2 represents warm water species *G. ruber*, *G. glutinata*, and *P. obliquiloculata* (Figs. 5 and 9), serving as a better proxy for Kuroshio intrusion into the OT, that further regulates the strength of the TWC. Same modern planktonic foraminifera assemblages also can be found in the surface sediments in the northern OT and Ryukyu Arc region, which is closely related with the Kuroshio (Thompson, 1981; Ujiie and Ujiie, 2000), ~~the average contents of *G. ruber* and *G. glutinata* are 18% and 28%, respectively. Though the foraminifera shells of *G. ruber*, *G. glutinata*, *G. sacculifer* and *G. conglobatus* are susceptible to carbonate dissolution (Thompson, 1981). *P. obliquiloculata*, another indicator species of Kuroshio strength, is very resistant to dissolution. The dominances of both dissolution-susceptible and resistant species in Factor 2 (Table 2) indicate no dissolution bias in the faunal signals.~~ We could thus infer that the higher scores of Factor 2 during MIS 5.1 and MIS 1 reflect stronger Kuroshio intrusion into the northern OT.

The faunal Factor 3 includes cold water species *N. pachyderma* (dex.) and *G. quinqueloba*, of which higher scores indicate increased influence of cold water intruding into the northern OT.

1 *N. pachyderma* (dex.) and *G. quinqueloba* mainly live in the Arctic and subarctic waters. In
 2 the modern surface sediments of the ECS, however, the abundance of *N. pachyderma* is very
 3 low (Xu and Oda, 1999). During 12.5-24 ka, the higher Factor 3 scores and abundances of *N.*
 4 *pachyderma* (dex.) (Figs. 5 and 9) along with low alkenone SST (Fig. 8) indicate strong
 5 invasion of cold water, which is related to the southward shift of subarctic front, and an abrupt
 6 northward shift by 12 ka. The higher abundances of *G. quinqueloba* in the surface sediments
 7 of the ECS are mainly limited in the Yangtze estuary region with low SSS and SST,
 8 indicating the influences of cold, low-salinity coastal water masses (Xu and Oda, 1999). High
 9 abundances of *G. quinqueloba* link to low SSS before 18 ka, and late MIS 3 and early MIS 4
 10 (Fig. 8), indicating an increased river runoff effect or increased precipitation versus
 11 evaporation in northern OT while the sea level was relatively lower. During the LGM and H
 12 events/stadials, the decreased abundances of *G. quinqueloba* correspond well with the
 13 increased SSS, which reflect stronger winter and/or weaker summer AMs.

14 Factor 4 is mainly composed of the species related with the DOT, including *G. inflata* and *N.*
 15 *dutertrei* (Bé, 1977). In the regions of Kuroshio and Taiwan Warm Current, the abundances
 16 of *N. dutertrei* in modern surface sediments are high to 20-40% (Wang et al., 1988). In the
 17 ECS and the northern OT, the high abundances of *N. dutertrei* in the surface sediments appear
 18 to be associated with ~~strong frontal~~transitional zones between Kuroshio and the coastal water
 19 (Li et al., 2007). In CSH1, high abundances of *N. dutertrei* correlate well with the shallower
 20 DOT (Fig. ~~6;~~9), suggesting that the Factor 4 scores and *N. dutertrei* abundances are
 21 indicative of nutrient and upwelling conditions. Though *G. inflata* is also a species indicative
 22 of strong ~~upwelling or~~ mixing Thompson (1981), in core CSH1, its abundances show no
 23 correlation with the DOT (Fig. ~~6;~~9). We consider that the abundances of *G. inflata* may
 24 respond to nutrient distributions (Cléroux et al., 2007), or more extreme or short-lived
 25 upwelling conditions that are not well captured by the DOT transfer function used in this
 26 study.

27 Our approach of combined $\delta^{18}\text{O}_{\text{ruber}}$ and alkenone SST for deconvoluting SSS (Fig. 8)
 28 indicates a modern value since ~8 ka, confirming the reliability of this estimation method.
 29 The local SSS in the northern OT is mainly regulated by two factors – river runoff ~~related to~~
 30 ~~AM precipitation~~ and oceanic high salinity water brought by the Kuroshio. The effects of both
 31 factors are constrained by the sea level. In addition, the upwelling may also bring saline water
 32 to the surface. In our CSH1 SSS record, the SSS values are ~2 psu higher than that of today

during MIS 5.1, ~~while. Considering that $\delta^{18}\text{O}_{\text{ruber}}$ in core CSH1 is controlled mainly by SST and SSS, we found that the SST difference between MIS 1 and MIS 5.1 is $\sim 0.3^\circ\text{C}$, which is translated into only $\sim 0.066\text{‰}$ as a temperature effect in driving $\delta^{18}\text{O}_{\text{ruber}}$ changes. However, the $\delta^{18}\text{O}_{\text{ruber}}$ difference between MIS 1 and MIS 5.1 is $\sim 0.74\text{‰}$, which is not possibly affected by temperature change. Therefore this observation suggests that the much heavier $\delta^{18}\text{O}_{\text{ruber}}$ in MIS 5.1 and whole CSH1 $\delta^{18}\text{O}_{\text{ruber}}$ record must be dominated by other factors, such as local SSS and regional precipitation versus evaporation.~~

This estimation, along with the higher abundances of *P. obliquiloculata* (Fig. 6), suggesting stronger intrusion of the Kuroshio into the northern OT. During the conditions of lowering sea levels, the saline Kuroshio water intrusions were weakened. As seen from the faunal records in late MIS 3 (Figs. 5 and 9), the increased CSH1 SSS values coincide with higher abundances of *G. bulloides* and Factor 1, which are strong indications for strong upwelling in the northern OT (Li et al., 2007). After 24–16 ka, though global sea level has been raised, the saline intrusion of Kuroshio might be counteracted by ~~very~~ fresh river runoff water ~~from and~~ increased regional precipitation brought by intensified summer AM (Wang et al., 2001; Wang et al., 2008; Yuan et al., 2004), resulting in low SSS conditions since then (Fig. 8). During the LGM and H events/stadials, the SSS values were significantly increased (Fig. 8). ~~The $\delta^{18}\text{O}$ of stalagmites in the East China showed w~~weakened summer AM ~~at the time~~ (Wang et al., 2001; Wang et al., 2008; Yuan et al., 2004), ~~that had caused~~ regional aridity and less precipitation/river runoff from Yangtze and Huanghe Rivers, ~~which~~ are responsible for the high saline water in the northern OT. ~~(Wang et al., 2001; Wang et al., 2008; Yuan et al., 2004)~~ (Fig. 11). In addition, the stronger winter AM during the cold episodes may have intensified the surface water mixing, which also helps increase the SSS.

Evidences from our CSH1 SSTs, SSSs, DOTs, and *P. obliquiloculata* abundances support the strength of the Kuroshio and the TWC had been responded to regional and global climate forcing since the last 88 ka. They are exemplified in the lower SST, SSS, shallower DOT, and lower abundances of *P. obliquiloculata*, which imply weakened Kuroshio intrusion into the northern OT during the LGM (Fig. 6; 8; 9). During MIS 1 and MIS 5.1, evidences of higher SST, SSS, and ~~low~~^{higher} abundances of *P. obliquiloculata* indicate strong Kuroshio intrusion. Low sea level conditions appear to block or decrease the intrusion of the Kuroshio into the OT. It is exemplified by the lower SST and lower abundances of *P. obliquiloculata* during MIS 3 and MIS 4 in comparing to MIS 1 and MIS 5.1. Our records show consistent

带格式的：字体：Times New Roman

带格式的：上标

域代码已更改

域代码已更改

evidence provided from core MD982195 (Ijiri et al., 2005) (Fig.1), indicating it is a robust regional pattern in the northern OT. Previous studies also suggest that the strength of Kuroshio had been weakened abruptly during the late Holocene (Jian et al., 2000a; Li et al., 1997; Shieh et al., 1997), a mysterious short-lived episode that may imply weakened Kuroshio. This event could be found in CSH1 (Fig. 6), suggesting that it is also a robust regional feature with more spatial scale in the main stream Kuroshio region. Despite of disputes between studies by the uses of paleoceanographic data or modeling approaches on whether or not the Kuroshio had intruded into the OT during glacial low sea level conditions (Ujiié and Ujiié, 1999; Ujiié et al., 2003), our evidence shows that the high SST and SSS conditions and Kuroshio indicative planktonic foraminifera had existed in at least one major branch of the Kuroshio in the northern OT. Though the volume transport of the Kuroshio responds to the trade wind (Sawada and Handa, 1998), ~~and that the barotropic forcing is a key for controlling the meandering mode of Kuroshio (Yasuda et al., 1985),~~ which may cause regional variability of Kuroshio intrusion into the OT, our multiproxy records show homogenous responses in the OT and suggest that the Kuroshio is the most dominant mechanism governing the hydrographic variations over the past 88 ka.

5.2 Millennial-scale responses of the Kuroshio

Our multiproxy hydrographic records present clear evidence for high frequency, millennial-scale fluctuations in the responses of the Kuroshio. The high frequency component in CSH1 $\delta^{18}\text{O}_{\text{ruber}}$ shares similar feature with foraminifer $\delta^{18}\text{O}$ in MD982195 (Ijiri et al., 2005) and GISP2 ice core $\delta^{18}\text{O}$ (Stuiver and Grootes, 2000). Our CSH1 alkenone SST show abrupt decreases and 3.5°C, 2.1°C, 1.5°C, 1.4°C and 1.7°C lower than modern values during the following short-term intervals: 15.8-17.1 ka, 24.3-26 ka, 29.9-31.6 ka, 37.3-39.5 ka, and 46.9-49.4 ka, respectively (Table 3) (Figs. ~~4 and 10~~8). Moreover, the average values of $\delta^{18}\text{O}_{\text{ruber}}$ during those periods are relatively heavier by 1.43‰, 1.65‰, 1.48‰, 1.59‰ and 1.15‰, respectively than ~~—~~that in the most recent ~~abrupt~~ cooling during ~8 ka (-2.12‰). The timing of the ~~abrupt~~ heavier events corresponds to the H events/stadial (Bond et al., 1992; Bond et al., 1999). During 12.8-15 ka, the increased SST and lighter $\delta^{18}\text{O}_{\text{ruber}}$ in CSH1 correspond well with the Bølling-Allerød warm period. During H events/stadials, the abundances of *N. pachyderma* were increased, while the warm water species, *G. ruber* and *G. sacculifer* were decreased (Fig. 6). Such similar millennial-scale hydrographic responses have been reported from marine core studies in the whole OT and stalagmite AM records from the East China (Li

et al., 2001; Wang et al., 2008) (Fig. 11). Taking all evidence together, we conclude that the millennial-scale oscillations are one of the robust, common responses in Kuroshio and AM dominant regions, and several mechanisms that invoke the teleconnection between the AM and the North Atlantic via the westerlies have been suggested earlier (Nagashima et al., 2011; Porter and An, 1995).

5.3 Orbital-scale responses of the Kuroshio

Precession forcing that changes the seasonal distributions of incoming solar insolation is a well-known in driving past monsoon variability. In core CSH1, the spectral analysis of $\delta^{18}\text{O}_{\text{ruber}}$, SST, SSS, DOT and the abundances of *G. ruber*, *P. obliquiloculata* and *N. pachyderma* (dex.) all shows a common frequency at the precession cycles (near 24 ka, ~~not shown~~ Fig.12), indicating precession forcing plays an important role in regulating the hydrographic changes in the northern OT.

Though the orbital-scale Kuroshio responses to the AM were identified in our spectral analysis on the hydrographic records, the controlling mechanisms on Kuroshio hydrographies are much more complicated than that interpreted solely based on an AM mechanism. For example, both SST and SSS values were high during MIS 5.1 (Fig.4+8). The average SST was close to the modern long-term instrumental observation value but the SSS was ~1.6 psu higher than today. While the summer AM is considered stronger during this specific episode, the high SSS and low abundances of coastal water species (Fig.8), *G. quinqueloba* suggest a reduced river runoff, which is in opposite to the condition of higher precipitation by enhanced summer AM. Moreover, during MIS 5.1, higher abundance of *P. obliquiloculata* suggests stronger Kuroshio (Fig. 6). In this context, we consider that the Kuroshio climate in MIS 5.1 is a warm but dry which is distinguishable from the other episodes in the western Pacific and East Asian paleoclimate(Ikehara and Oshima, 2009; Morley et al., 1991; Sun et al., 2003).

During MIS 4, the sea level was lowered and make the CSH1 site closer to the coastal line (Cutler et al., 2003) (Fig.11). Increased river runoff had caused decreased SSS values and the increased abundances of coastal water species *G. quinqueloba* during this time interval, while the abundances of *P. obliquiloculata* remained low, indicating a weakened Kuroshio intrusion. In particular, during MIS 4.2, the abundances of *G. quinqueloba* were decreased, corresponding well with the increased SSS. The Chinese loess grain size (> 32 μm) indicated that the winter AM was intensified during MIS 4.2 (Guo et al., 2009) (Fig. 11) and echoed the

带格式的: 字体颜色: 红色

scenario reconstructed here. In addition, during MIS 4 the higher abundances of *N. pachyderma* indicate a southward migration of subarctic water, suggesting coherent atmospheric and oceanic changes in responding to Northern Hemispheric cooling ~~at this time.~~

Our alkenone SST and SSS reached maxima during early MIS 3 (~50 ka) and mid-MIS 3 (~35 ka) and rapidly decreased since ~35 ka (Fig. 8). However, lower abundances of *P. obliquiloculata* during MIS 3 suggest a weakened Kuroshio intrusion, which may have been caused by a partial blocking of gateways into the OT in relative low sea level condition during this time. ~~This is also in opposite to the conditions reconstructed from our SST and SSS, which could be used to infer a stronger Kuroshio intrusion at this time.~~ The MIS 3 climate was interrupted by several millennial-scale, high abundance episodes of *N. pachyderma* and *G. inflata*, indicating rapid ~~latitudinal shifting of the subarctic front during MIS 3~~ cooling of surface sea water (Fig. 6). ~~The increased abundances of the upwelling species *G. bulloides* and Factor 1 scores suggested that the~~ We speculate that the MIS 3 MIS 3 climate was characterized by a strengthened ~~summer-winter~~ AM, ~~as evidenced from the increased abundances of the upwelling species *G. bulloides* and Factor 1 scores~~ (Fig. 6; 10), with more frequent southward shifting of subarctic front, and weakened Kuroshio intrusion into the northern OT mainly due to lower sea level.

During MIS 2, high abundances of *N. pachyderma* (dex.) suggest a southward shift of subarctic frontal zone, resulting in low alkenone SST and SSS (Fig. 8). The DOT was much shallower, an indication for the reduced heat content in the surface water of the Kuroshio in the northern OT. After 16 ka, the abundances of *P. obliquiloculata* together with other warm water species, such as *G. ruber*, were gradually increased with the rise of sea level, indicating an intensified Kuroshio intrusion. During the LGM and H1, while Northern Hemispheric climate was very cold, our CSH1 SST and SSS were both decreased. This combination of hydrographic conditions indicates a ~~dominant weakened Kuroshio, which response to the high latitudinal cooling. Weakened Kuroshio intrusion into the OT could be driven by stronger boreal cooling as the Kuroshio~~ may have been diverted into the open northwestern Pacific at lower latitudes. The hydrographic conditions during the LGM and H1 appear to be not well explained by the AM, as weakened summer AM at these cold intervals would cause low SST and high SSS, which are inconsistent with our reconstructions.

Since 12 ka, while global climate has continued much warmer conditions, our SST values are increased, responding to the rise of sea level and stronger intrusion of the Kuroshio into the

northern OT. The stronger Kuroshio in responding to rising sea level is evidence by higher abundances of warm water species and of *P. obliquiloculata*. The lower abundances of *G. quinqueloba* indicate a reduced influence of coastal water since 12 ka. The abundances of *N. pachyderma* (dex) have been decreased abruptly, indicating a rapid northward shift of subarctic frontal zone. Therefore, our reconstruction supports that the Kuroshio is the main factor that controls the hydrographic evolution in the northern OT since 12 ka.

6 Conclusions

Based on AMS ^{14}C and $\delta^{18}\text{O}$ correlation, a new high resolution hydrographic record was firstly established with an extension down to 88 ka in the northern OT. Multiproxies, including alkenone SST, $\delta^{18}\text{O}$ deconvoluted-SSS, planktonic foraminiferal assemblages, and the DOT from core CSH1, suggest that the hydrography in the surface water in the OT is a homogenous system that has responded dramatically mainly to the global sea level, Northern Hemispheric climate, and regional mechanisms such as the Kuroshio, AM and subarctic front. The main conclusions are as following:

(1) The surface hydrologic variability in the northern OT of the past 88 ka shows sensitive responses to the abrupt climate changes. During MIS 1 and MIS 5.1, the surface hydrology was dominated by the Kuroshio while sea level was relatively high. During MIS 2, 3 and 4, however, stronger winter AM and southward mean position of the subarctic front played more important roles in governing the hydrographic conditions.

(2) On millennial time scales, five abrupt events with decreased SSTs and increased SSS corresponding to the timing of Heinrich events were identified in CSH1 hydrographic records. We identified these abrupt events as responses to relatively weaker summer AM which may link to a tight teleconnection between the AM and the North Atlantic via the changes in the strength of the westerlies.

(3) All proxies show a common frequency near the precession cycles, suggesting an important monsoon-controlled mechanism in the surface water in the OT. During MIS 5.1, the ocean climate in the northern OT was warm but dry which was distinguishable from the other episodes in the western Pacific and East Asian paleoclimate. During MIS 4 and MIS 2, the ocean climate was dry and cold, which are thought to be mainly regulated by stronger winter AM and southwardly shifts of the subarctic front. During MIS 3, the ocean climate was

1 characterized by a strengthened summer AM but interrupted by millennial-scale cooling
2 events, indicating a rapid latitudinal shifting of the subarctic front, and weakened Kuroshio
3 intrusion into the northern OT. During MIS 1, the Kuroshio has returned back as a main factor
4 that controls the hydrographic evolution in the northern OT.

6 **Acknowledgements**

7 This study was supported by the National Natural Science Foundation of China (Grant No.:
8 40710069004, 40431002, 41206059, 41221004), by Basic Scientific Fund for National Public
9 Research Institutes of China (No.: 2012G31, GY0213G23) and by the Youth Foundation of
10 the State Oceanic Administration People's Republic of China (2012301). We thank Yoshiaki
11 Saito (Geological survey of Japan) for helping the determination of reflectance of volcanic
12 glass.

References

- Anderson, D. M. and Prell, W. L.: A 300 KYR Record of Upwelling Off Oman during the Late Quaternary: Evidence of the Asian Southwest Monsoon, *Paleoceanography*, 8, 193-208, 1993.
- Andreasen, D. J. and Ravelo, A. C.: Tropical Pacific Ocean thermocline depth reconstructions for the Last Glacial Maximum, *Paleoceanography*, 12, 395-413, 1997.
- Bé, A. W. H.: An ecological, zoogeographic and taxonomic review of recent planktonic foraminifera. In: *Oceanic Micropaleontology*, Ramsay, A. T. S. (Ed.), Academic Press, London, 1977.
- Berger, A. and Loutre, M. F.: Insolation values for the climate of the last 10 million years, *Quaternary Science Reviews*, 10, 297-317, 1991.
- Bintanja, R., van de Wal, R. S. W., and Oerlemans, J.: Modelled atmospheric temperatures and global sea levels over the past million years, *Nature*, 437, 125-128, 2005.
- Bond, G., Heinrich, H., Broecker, W., Labeyrie, L., McManus, J., Andrews, J., Huon, S., Jantschik, R., Clasen, S., and Simet, C.: Evidence for massive discharges of icebergs into the North Atlantic ocean during the last glacial period, *Nature*, 360, 245-249, 1992.
- Bond, G. C., Showers, W., Elliot, M., Evans, M., Lotti, R., Hajdas, I., Bonani, G., and Johnson, S.: The North Atlantic's 1-2 Kyr Climate Rhythm: Relation to Heinrich Events, Dansgaard/Oeschger Cycles and the Little Ice Age. In: *Mechanisms of Global Climate Change at Millennial Time Scales*, Clark, P. U., Webb, R. S., and Keigwin, L. D. (Eds.), American Geophysical Union, 1999.
- Buhring, C.: East Asian Monsoon variability on orbital- and millennial-to-sub-decadal time scales, Ph.D thesis, University of Kiel, 164 pp., 2001.
- Chang, Y.-P., Wang, W.-L., and Chen, M.-T.: The last 100 000 years' palaeoenvironmental changes inferred from the diatom assemblages of core MD012404 from the Okinawa Trough, East China Sea, *Journal of Quaternary Science*, 24, 890-901, 2009.
- Chang, Y. P., Wang, W. L., Yokoyama, Y., Matsuzaki, H., Kawahata, H., and Chen, M. T.: Millennial-scale planktic foraminifer faunal variability in the East China Sea during the past 40000 years (IMAGES MD012404 from the Okinawa Trough), *Terrestrial Atmospheric and Oceanic Sciences*, 19, 389-401, 2008.
- Chen, J., Zhang, D., Zhang, W., and Li, T.: The paleoclimatic change since the last glacialiation in the north of Okinawa Trough based on the spore-pollen records, *Acta Oceanologica Sinica*, 28, 85-91(in Chinese with English Abstract), 2006.
- Chen, M.-T., Shiau, L.-J., Yu, P.-S., Chiu, T.-C., Chen, Y.-G., and Wei, K.-Y.: 500 000-Year records of carbonate, organic carbon, and foraminiferal sea-surface temperature from the southeastern South China Sea (near Palawan Island), *Palaeogeography, Palaeoclimatology, Palaeoecology*, 197, 113-131, 2003.
- Cléroux, C., Cortijo, E., Duplessy, J.-C., and Zahn, R.: Deep-dwelling foraminifera as thermocline temperature recorders, *Geochemistry, Geophysics, Geosystems*, 8, Q04N11, doi:10.1029/2006GC001474, 2007.
- Coplen, T. B.: Calibration of the calcite-water oxygen-isotope geothermometer at Devils Hole, Nevada, a natural laboratory, *Geochimica et Cosmochimica Acta*, 71, 3948-3957, 2007.
- Cutler, K. B., Edwards, R. L., Taylor, F. W., Cheng, H., Adkins, J., Gallup, C. D., Cutler, P. M., Burr, G. S., and Bloom, A. L.: Rapid sea-level fall and deep-ocean temperature change since the last interglacial period, *Earth and Planetary Science Letters*, 206, 253-271, 2003.
- Du, J.-Q., Chen, M., Cao, J.-P., Qiu, Y.-S., Tong, J.-L., Ma, Q., and Yang, J.-H.: Oxygen isotope in seawater and its hydrological implication in the southern Yellow Sea and the East China Sea, *Oceanologia et Limnologia Sinica*, 43, 1057-1066(in Chinese with English Abstract), 2012.
- Emeis, K.-C., Anderson, D. M., Doose, H., Kroon, D., and Schulz-Bull, D.: Sea-Surface Temperatures and the History of Monsoon Upwelling in the Northwest Arabian Sea during the Last 500,000 Years, *Quaternary Research*, 43, 355-361, 1995.
- Ge, S., Shi, X., Wu, Y., Lee, T., Xiong, Y., and Saito, Y.: Rock magnetic property of gravity core CSH1 from the northern Okinawa Trough and the effect of early diagenesis, *Acta Oceanologica Sinica*, 26, 54-65, 2007.
- Guo, Z. T., Berger, A., Yin, Q. Z., and Qin, L.: Strong asymmetry of hemispheric climates during MIS-13 inferred from correlating China loess and Antarctica ice records, *Clim. Past*, 5, 21-31, 2009.
- Hemleben, C., Spindler, M., and Anderson, O. R.: *Modern planktonic foraminifera*, Springer, Berlin, 1989.
- Hsueh, Y.: The Kuroshio in the East China Sea, *Journal of Marine Systems*, 24, 131-139, 2000.
- Hsueh, Y., Wang, J., and Chern, C. S.: The Intrusion of the Kuroshio across the continental-shelf northeast of Taiwan, *Journal of Geophysical Research-Oceans*, 97, 14323-14330, 1992.
- Ijiri, A., Wang, L. J., Oba, T., Kawahata, H., and Huang, C. Y.: Paleoenvironmental changes in the northern area of the East China Sea during the past 42,000 years, *Palaeogeography Palaeoclimatology Palaeoecology*, 219, 239-261, 2005.
- Ikehara, K. and Oshima, H.: Orbital- and millennial-scale fluctuations in late Quaternary marine pollen records from the Japan Sea, *Journal of Quaternary Science*, 24, 866-879, 2009.

Jian, Z., Wang, P., Saito, Y., Wang, J., Pflaumann, U., Oba, T., and Cheng, X.: Holocene variability of the Kuroshio Current in the Okinawa Trough, northwestern Pacific Ocean, *Earth and Planetary Science Letters*, 184, 305-319, 2000a.

Jian, Z. M., Li, B. H., Huang, B. Q., and Wang, J. L.: Globorotalia truncatulinoides as indicator of upper-ocean thermal structure during the Quaternary: evidence from the South China Sea and Okinawa Trough, *Palaeogeography Palaeoclimatology Palaeoecology*, 162, 287-298, 2000b.

Jian, Z. M., Saito, Y., Wang, P. X., Li, B. H., and Chen, R. H.: Shifts of the Kuroshio axis over the last 20,000 years, *Chinese Science Bulletin*, 43, 1053-1056, 1998.

Kao, S. J., Roberts, A. P., Hsu, S. C., Chang, Y. P., Lyons, W. B., and Chen, M. T.: Monsoon forcing, hydrodynamics of the Kuroshio Current, and tectonic effects on sedimentary carbon and sulfur cycling in the Okinawa Trough since 90 ka, *Geophysical Research Letters*, 33, doi:10.1029/2005gl025154, 2006a.

Kao, S. J., Wu, C.-R., Hsin, Y.-C., and Dai, M.: Effects of sea level change on the upstream Kuroshio Current through the Okinawa Trough, *Geophysical Research Letters*, 33, L16604, doi:10.1029/2006gl026822, 2006b.

Kawahata, H., Nohara, M., Aoki, K., Minoshima, K., and Gupta, L. P.: Biogenic and abiogenic sedimentation in the northern East China Sea in response to sea-level change during the Late Pleistocene, *Global and Planetary Change*, 53, 108-121, 2006.

Kubota, Y., Kimoto, K., Tada, R., Oda, H., Yokoyama, Y., and Matsuzaki, H.: Variations of East Asian summer monsoon since the last deglaciation based on Mg/Ca and oxygen isotope of planktic foraminifera in the northern East China Sea, *Paleoceanography*, 25, PA4205, doi:10.1029/2009pa001891, 2010.

Lee, C.-S., Shor Jr, G. G., Bibee, L. D., Lu, R. S., and Hilde, T. W. C.: Okinawa Trough: Origin of a back-arc basin, *Marine Geology*, 35, 219-241, 1980.

Lee, K. E., Lee, H. J., Park, J.-H., Chang, Y.-P., Ikehara, K., Itaki, T., and Kwon, H. K.: Stability of the Kuroshio path with respect to glacial sea level lowering, *Geophysical Research Letters*, 40, 392-396, doi:10.1002/grl.50102, 2013.

Li, B. H., Jian, Z. M., and Wang, P. X.: Pulleniatina obliquiloculata as a paleoceanographic indicator in the southern Okinawa Trough during the last 20,000 years, *Marine Micropaleontology*, 32, 59-69, 1997.

Li, T., Liu, Z., Hall, M. A., Saito, Y., Berne, S., Cang, S., and Cheng, Z.: A broad deglacial $\delta^{13}\text{C}$ minimum event in planktonic foraminiferal records in the Okinawa Trough, *Chinese Science Bulletin*, 47, 599-603, 2002.

Li, T. G., Liu, Z. X., Hall, M. A., Berne, S., Saito, Y., Cang, S. X., and Cheng, Z. B.: Heinrich event imprints in the Okinawa Trough: evidence from oxygen isotope and planktonic foraminifera, *Palaeogeography Palaeoclimatology Palaeoecology*, 176, 133-146, 2001.

Li, T. G., Sun, R. T., Zhang, D. Y., Liu, Z. X., Li, Q., and Jiang, B.: Evolution and variation of the Tsushima warm current during the late Quaternary: Evidence from planktonic foraminifera, oxygen and carbon isotopes, *Science in China Series D-Earth Sciences*, 50, 725-735, 2007.

Lie, H.-J. and Cho, C.-H.: Recent advances in understanding the circulation and hydrography of the East China Sea, *Fisheries Oceanography*, 11, 318-328, 2002.

Lie, H. J., Cho, C. H., Lee, J. H., and Lee, S.: Structure and eastward extension of the Changjiang River plume in the East China Sea, *Journal of Geophysical Research: Oceans*, 108, doi:10.1029/2001JC001194, 2003.

Liu, Z. X., Li, T. G., Li, P. Y., Huang, Q. Y., Berne, S., Saito, Y., Cheng, Z. B., Wei, G. J., Liu, L. J., and Li, Z.: The paleoclimatic events and cause in the Okinawa Trough during 50 kaBP, *Chinese Science Bulletin*, 46, 153-157, 2001.

Machida, H.: The stratigraphy, chronology and distribution of distal marker-tephras in and around Japan, *Global and Planetary Change*, 21, 71-94, 1999.

Martinson, D. G., Pisias, N. G., Hays, J. D., Imbrie, J., Moore, T. C., and Shackleton, N. J.: Age dating and the orbital theory of the ice ages: Development of a high-resolution 0 to 300,000-year chronostratigraphy, *Quaternary Research*, 27, 1-29, 1987.

Morley, J. J., Heusser, L. E., and Shackleton, N. J.: Late Pleistocene/Holocene radiolarian and pollen records from sediments in the Sea of Okhotsk, 6, 121-131, 1991.

Mulitza, S., Arz, H., Kemle-von Mücke, S., Moos, C., Niebler, H. S., Pätzold, J., and Segl, M.: The South Atlantic Carbon Isotope Record of Planktic Foraminifera. In: *Use of Proxies in Paleoceanography*, Fischer, G. and Wefer, G. (Eds.), Springer Berlin Heidelberg, 1999.

Mulitza, S., Donner, B., Fischer, G., Paul, A., Pätzold, J., Rühlemann, C., and Segl, M.: The South Atlantic Oxygen Isotope Record of Planktic Foraminifera. In: *The South Atlantic in the Late Quaternary*, Wefer, G., Mulitza, S., and Ratmeyer, V. (Eds.), Springer Berlin Heidelberg, 2004.

Muller, P. J., Kirst, G., Ruhland, G., von Storch, I., and Rosell-Mele, A.: Calibration of the alkenone paleotemperature index U_{37}^K based on core-tops from the eastern South Atlantic and the global ocean (60 degrees N-60 degrees S), *Geochimica et Cosmochimica Acta*, 62, 1757-1772, 1998.

Nagashima, K., Tada, R., Tani, A., Sun, Y., Isozaki, Y., Toyoda, S., and Hasegawa, H.: Millennial-scale

oscillations of the westerly jet path during the last glacial period, *Journal of Asian Earth Sciences*, 40, 1214-1220, 2011.

Nakanishi, T., Yamamoto, M., Irino, T., and Tada, R.: Distribution of glycerol dialkyl glycerol tetraethers, alkenones and polyunsaturated fatty acids in suspended particulate organic matter in the East China Sea, *Journal of Oceanography*, 68, 959-970, 2012.

Oba, T.: Paleooceanographic information obtained by the isotopic measurement of individual foraminiferal specimens, 1988, 169-180, 1988.

Peeters, F. J. C., Brummer, G.-J. A., and Ganssen, G.: The effect of upwelling on the distribution and stable isotope composition of *Globigerina bulloides* and *Globigerinoides ruber* (planktic foraminifera) in modern surface waters of the NW Arabian Sea, *Global and Planetary Change*, 34, 269-291, 2002.

Pflaumann, U., Duprat, J., Pujol, C., and Labeyrie, L. D.: SIMMAX: A modern analog technique to deduce Atlantic sea surface temperatures from planktonic foraminifera in deep-sea sediments, *Paleoceanography*, 11, 15-35, 1996.

Pflaumann, U. and Jian, Z.: Modern distribution patterns of planktonic foraminifera in the South China Sea and western Pacific: a new transfer technique to estimate regional sea-surface temperatures, *Marine Geology*, 156, 41-83, 1999.

Porter, S. C. and An, Z.: Correlation between climate events in the North Atlantic and China during the last glaciation, *Nature*, 375, 305-308, 1995.

Ravelo, A. C. and Fairbanks, R. G.: Oxygen Isotopic Composition of Multiple Species of Planktonic Foraminifera: Records of the Modern Photoc Zone Temperature Gradient, *Paleoceanography*, 7, 815-831, 1992.

Ravelo, A. C., Fairbanks, R. G., and Philander, S. G. H.: Reconstructing tropical Atlantic hydrography using planktonic foraminifera and an ocean model, *Paleoceanography*, 5, 409-431, 1990.

Reimer, P. J., Baillie, M. G. L., Bard, E., Bayliss, A., Beck, J. W., Blackwell, P. G., Ramsey, C. B., Buck, C. E., Burr, G. S., Edwards, R. L., Friedrich, M., Grootes, P. M., Guilderson, T. P., Hajdas, I., Heaton, T. J., Hogg, A. G., Hughen, K. A., Kaiser, K. F., Kromer, B., McCormac, F. G., Manning, S. W., Reimer, R. W., Richards, D. A., Southon, J. R., Talamo, S., Turney, C. S. M., van der Plicht, J., and Weyhenmeyer, C. E.: Intcal09 and Marine09 Radiocarbon age calibration curves, 0-50,000 years Cal BP, *Radiocarbon*, 51, 1111-1150, 2009.

Sawada, K. and Handa, N.: Variability of the path of the Kuroshio ocean current over the past 25,000 years, *Nature*, 392, 592-595, 1998.

Shieh, Y. T., Wang, C. H., Chen, M. P., and Yung, Y. L.: The Last Glacial Maximum to Holocene environment changes in the southern Okinawa Trough, *Journal of Asian Earth Sciences*, 15, 3-8, 1997.

Sibuet, J. C., Letouzey, J., Barbier, F., Charvet, J., Foucher, J. P., Hilde, T. W. C., Kimura, M., Chiao, L.-Y., Marsset, B., Muller, C., and Stéphan, J. F.: Back Arc Extension in the Okinawa Trough, *Journal of Geophysical Research: Solid Earth*, 92, 14041-14063, 1987.

Stuiver, M. and Grootes, P. M.: GISP2 Oxygen Isotope Ratios, *Quaternary Research*, 53, 277-284, 2000.

Sun, X., Luo, Y., Huang, F., Tian, J., and Wang, P.: Deep-sea pollen from the South China Sea: Pleistocene indicators of East Asian monsoon, *Marine Geology*, 201, 97-118, 2003.

Sun, Y. B., Oppo, D. W., Xiang, R., Liu, W. G., and Gao, S.: Last deglaciation in the Okinawa Trough: Subtropical northwest Pacific link to Northern Hemisphere and tropical climate, *Paleoceanography*, 20, 2005.

Tanaka, Y.: Coccolith fluxes and species assemblages at the shelf edge and in the Okinawa Trough of the East China Sea, *Deep Sea Research Part II: Topical Studies in Oceanography*, 50, 503-511, 2003.

Thompson, P. R.: Planktonic foraminifera in the Western North Pacific during the past 150 000 years: Comparison of modern and fossil assemblages, *Palaeogeography, Palaeoclimatology, Palaeoecology*, 35, 241-279, 1981.

Thunell, R. C., Curry, W. B., and Honjo, S.: Seasonal variation in the flux of planktonic foraminifera: time series sediment trap results from the Panama Basin, *Earth and Planetary Science Letters*, 64, 44-55, 1983.

Ujiié, H. and Ujiié, Y.: Late Quaternary course changes of the Kuroshio Current in the Ryukyu Arc region, northwestern Pacific Ocean, *Marine Micropaleontology*, 37, 23-40, 1999.

Ujiié, Y., Ujiié, H., Taira, A., Nakamura, T., and Oguri, K.: Spatial and temporal variability of surface water in the Kuroshio source region, Pacific Ocean, over the past 21,000 years: evidence from planktonic foraminifera, *Marine Micropaleontology*, 49, 335-364, 2003.

Ujiié, Y. and Ujiié, H.: Distribution and oceanographic relationships of modern planktonic foraminifera in the Ryukyu arc region, northwest Pacific Ocean, *The Journal of Foraminiferal Research*, 30, 336-360, 2000.

Wang, P. X., Zhang, J. J., and Zhao, Q. H.: Foraminifera and Ostracoda in sediments in the East China Sea (in Chinese), China Ocean Press, Beijing 1988.

Wang, Y., Cheng, H., Edwards, R. L., An, Z., Wu, J., Shen, C.-C., and Dorale, J. A.: A High-Resolution Absolute-Dated Late Pleistocene Monsoon Record from Hulu Cave, China, *Science*, 294, 2345-2348, 2001.

Wang, Y., Cheng, H., Edwards, R. L., Kong, X., Shao, X., Chen, S., Wu, J., Jiang, X., Wang, X., and An, Z.: Millennial- and orbital-scale changes in the East Asian monsoon over the past 224,000 years, *Nature*, 451, 1090-

1093, 2008.

Watanabe, M.: Simulation of temperature, salinity and suspended matter distributions induced by the discharge into the East China Sea during the 1998 flood of the Yangtze River, *Estuarine Coastal and Shelf Science*, 71, 81-97, 2007.

Wu, Y., Cheng, Z., and Shi, X.: Stratigraphic and carbonate sediment characteristics of Core CSH1 from the northern Okinawa Trough, *Advances in Marine Science*, 22, 163-169(in Chinese with English Abstract), 2004.

Xiang, R., Sun, Y. B., Li, T. G., Oppo, D. W., Chen, M. H., and Zheng, F.: Paleoenvironmental change in the middle Okinawa Trough since the last deglaciation: Evidence from the sedimentation rate and planktonic foraminiferal record, *Palaeogeography Palaeoclimatology Palaeoecology*, 243, 378-393, 2007.

Xing, L., Zhao, M., Zhang, H., Liu, Y., and Shi, X.: Biomarker reconstruction of phytoplankton productivity and community structure changes in the middle Okinawa Trough during the last 15 ka, *Chinese Science Bulletin*, 53, 2552-2559, 2008.

Xu, X. D. and Oda, M.: Surface-water evolution of the eastern East China Sea during the last 36,000 years, *Marine Geology*, 156, 285-304, 1999.

Yasuda, I., Yoon, J.-H., and Sugimoto, N.: Dynamics of the Kuroshio large meander, *Journal of the Oceanographical Society of Japan*, 41, 259-273, 1985.

Yu, H., Liu, Z. X., Berne, S., Jia, G. D., Xiong, Y. Q., Dickens, G. R., Wei, G. J., Shi, X. F., Liu, J. P., and Chen, F. J.: Variations in temperature and salinity of the surface water above the middle Okinawa Trough during the past 37 kyr, *Palaeogeography Palaeoclimatology Palaeoecology*, 281, 154-164, 2009.

Yuan, D., Cheng, H., Edwards, R. L., Dykoski, C. A., Kelly, M. J., Zhang, M., Qing, J., Lin, Y., Wang, Y., Wu, J., Dorale, J. A., An, Z., and Cai, Y.: Timing, Duration, and Transitions of the Last Interglacial Asian Monsoon, *Science*, 304, 575-578, 2004.

Zhang, J., Letolle, R., Martin, J. M., Jussierand, C., and Mouchel, J. M.: Stable oxygen isotope distribution in the Huanghe (Yellow River) and the Changjiang (Yangtze River) estuarine systems, *Continental Shelf Research*, 10, 369-384, 1990.

Zhou, H., Li, T., Jia, G., Zhu, Z., Chi, B., Cao, Q., Sun, R., and Peng, P. a.: Sea surface temperature reconstruction for the middle Okinawa Trough during the last glacial-interglacial cycle using C-37 unsaturated alkenones, *Palaeogeography Palaeoclimatology Palaeoecology*, 246, 440-453, 2007.

1 Table 1. Details of age controlling points of accelerator mass spectrometry radiocarbon (AMS
2 ^{14}C) and $\delta^{18}\text{O}$ of planktonic foraminifera in core CSH1 used for age model reconstruction.

| Depth | Materials | AMS ^{14}C | Error (yr) | Range($\delta\delta$) | Calibrated age | Sedimentation rate | Source |
|-------|---------------------|---------------------|------------|-------------------------|----------------|--------------------|--------------------|
| (cm) | | (yr) | | (cal yr BP) | (cal yr BP) | (cm ka $^{-1}$) | |
| 10 | <i>N. dutertrei</i> | 3420 | ± 35 | 3261-3339 | 3301 | | this study |
| 106 | <i>N. dutertrei</i> | 7060 | ± 40 | 7500-7580 | 7542 | 22.6 | this study |
| 150 | <i>N. dutertrei</i> | 10840 | ± 50 | 12220-12392 | 12328 | 9.2 | this study |
| 318 | <i>N. dutertrei</i> | 15130 | ± 80 | 17718-18029 | 17913 | 30.1 | Chen et al. (2006) |
| 362 | mixing species | 16990 | ± 140 | 19476-19510 | 19746 | 24.0 | Chen et al. (2006) |
| 558 | <i>N. dutertrei</i> | 20650 | ± 120 | 23975-24339 | 24161 | 44.4 | this study |
| 678 | mixing species | 22430 | ± 240 | 26084-26805 | 26472 | 51.9 | Chen et al. (2006) |
| 742 | <i>N. dutertrei</i> | 25440 | ± 210 | 29644-29746 | 29904 | 18.6 | this study |
| 850 | <i>N. dutertrei</i> | 27810 | ± 290 | 31283-31789 | 31572 | 64.7 | this study |
| 1002 | mixing species | 34050 | ± 850 | 37152-39359 | 38414 | 22.2 | Chen et al. (2006) |
| 1058 | MIS 3.13 | | ± 4710 | | 43 880 | 10.2 | this study |
| 1210 | MIS 3.3 | | ± 3850 | | 50 200 | 24.1 | this study |
| 1282 | MIS 3.31 | | ± 5030 | | 55 450 | 13.7 | this study |
| 1346 | MIS 4.22 | | ± 6350 | | 64 090 | 7.4 | this study |
| 1530 | MIS 5 | | ± 2590 | | 73 910 | 18.7 | this study |
| 1610 | MIS 5.1 | | ± 3580 | | 79 250 | 15.0 | this study |

1 Table 2. Descriptive statistics of planktonic foraminiferal species and Q-mode VARIMAX
2 factor analysis for core CSH1.

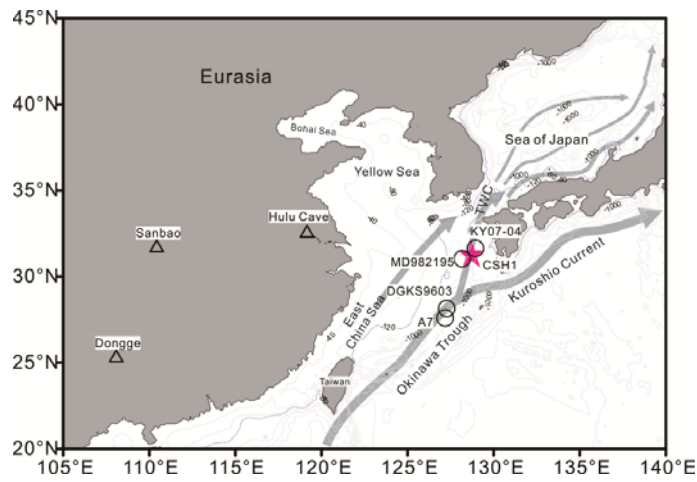
| | Max(%) | Min(%) | Average(%) | Stdev(%) | F1 | F2 | F3 | F4 |
|--|--------|--------|------------|----------|-------------|-------------|-------------|-------------|
| <i>Orbulina universa</i> | 1.57 | 0 | 0.24 | 0.26 | 0.03 | 0.16 | 0.05 | 0.29 |
| <i>Globigerinoides conglobatus</i> | 1.03 | 0 | 0.1 | 0.17 | -0.05 | 0.51 | -0.16 | 0.17 |
| <i>Globigerinoides ruber</i> | 22.34 | 5.25 | 11.59 | 3.28 | 0.10 | 0.94 | 0.01 | 0.14 |
| <i>Globigerinoides tenellus</i> | 3.52 | 0 | 1.04 | 0.66 | 0.09 | 0.71 | 0.09 | -0.03 |
| <i>Globigerinoides sacculifer</i> | 5.35 | 0.17 | 1.7 | 1.14 | -0.04 | 0.54 | -0.22 | 0.17 |
| <i>Globigerinella aequilateralis</i> | 2.62 | 0 | 0.37 | 0.42 | -0.03 | 0.43 | -0.32 | 0.15 |
| <i>Gloigerina calida</i> | 2.82 | 0 | 0.68 | 0.61 | -0.06 | 0.47 | -0.28 | 0.11 |
| <i>Globigerina bulloides</i> | 53.79 | 9.4 | 22.4 | 7.93 | 0.98 | 0.13 | 0.17 | -0.05 |
| <i>Globigerina falconensis</i> | 5.38 | 0 | 1.39 | 1.19 | -0.01 | 0.10 | 0.05 | 0.14 |
| <i>Globigerina digitata</i> | 0.4 | 0 | 0.01 | 0.05 | -0.03 | 0.18 | -0.15 | -0.01 |
| <i>Globigerinoides rubescens</i> | 2.22 | 0 | 0.68 | 0.5 | 0.20 | 0.71 | 0.09 | -0.05 |
| <i>Globigerina quinqueloba</i> | 8.86 | 0 | 2.34 | 1.43 | 0.11 | 0.32 | 0.58 | -0.08 |
| <i>Neogloboquadrina pachyderma(sin.)</i> | 0.67 | 0 | 0.1 | 0.14 | 0.01 | -0.14 | 0.45 | 0.04 |
| <i>Neogloboquadrina pachyderma(dex.)</i> | 25.89 | 0.14 | 10.49 | 5.8 | -0.08 | -0.20 | 0.96 | 0.16 |
| <i>N dutertrei</i> | 34.52 | 8.28 | 21.59 | 5.69 | 0.07 | 0.13 | 0.44 | 0.88 |
| <i>Globquadrina conglomerata</i> | 0.67 | 0 | 0.02 | 0.08 | -0.11 | -0.01 | 0.10 | 0.07 |
| <i>Pulleniatina obliquiloculata</i> | 6.79 | 0 | 1.8 | 1.45 | 0.00 | 0.62 | -0.40 | 0.38 |
| <i>Globorotalia inflata</i> | 11.26 | 0.18 | 4.9 | 2.64 | -0.11 | -0.03 | -0.05 | 0.52 |
| <i>Globorotalia truncatulinoides(sin.)</i> | 0.73 | 0 | 0.05 | 0.12 | -0.06 | -0.07 | -0.10 | 0.34 |
| <i>Globorotalia truncatulinoides(dex.)</i> | 2.04 | 0 | 0.27 | 0.35 | 0.04 | -0.15 | 0.32 | 0.01 |
| <i>Globorotalia crassaformis</i> | 5.74 | 0 | 0.95 | 0.76 | 0.02 | 0.33 | -0.09 | 0.05 |
| <i>Globorotalia menardii</i> | 1.11 | 0 | 0.17 | 0.23 | 0.04 | 0.33 | -0.35 | 0.32 |
| <i>Globigerinita glutinata</i> | 25.03 | 1.08 | 6.99 | 5.05 | 0.16 | 0.95 | -0.17 | -0.15 |
| % of Variance | | | | | 44.84 | 22.88 | 15.73 | 12.28 |
| Cumulative % | | | | | 44.84 | 67.72 | 83.46 | 95.74 |

3 Note: High factor loading (bold type) indicates the primary species contributing to each factor
4

1 Table 3. Average SST and SSS from proxies of different periods for core CSH1 and from
2 instrumental records in the study area around 28 - 29°N, 131 - 132°E.

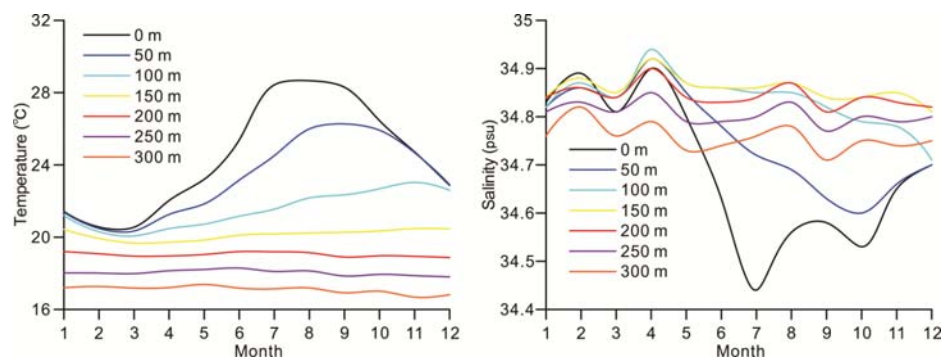
| | T(°C)* | S(PSU)* | | T(°C) | S(PSU) | | T(°C) | S(PSU) | | T(°C) | S(PSU) |
|---------|-------------|-------------|---------|-------|--------|-----|-------|--------|----|-------|--------|
| January | 21.43±0.83 | 34.83±0.08 | MIS 1 | 24.47 | 34.80 | PB | 24.13 | 35.02 | H2 | 22.4 | 35.72 |
| April | 22.03±1.33 | 34.90±0.12 | MIS 2 | 21.75 | 34.78 | YD | 22.64 | 35.21 | H3 | 23.08 | 36.16 |
| July | 28.43 ±1.08 | 34.44±0.2 | MIS 3 | 23.15 | 35.83 | BA | 22.06 | 35.12 | H4 | 23.11 | 36.66 |
| October | 26.45±1 | 34.53±0.12 | MIS 4 | 22.02 | 35.20 | H1 | 21.06 | 34.00 | H5 | 22.88 | 35.32 |
| Annual | 24.54±3.16 | 34.68 ±0.19 | MIS 5.1 | 24.33 | 36.42 | LGM | 21.5 | 34.64 | | | |

3 Note: data (*) obtained from Japan Oceanographic Data Center database,
4 <http://www.jodc.go.jp/service.htm>



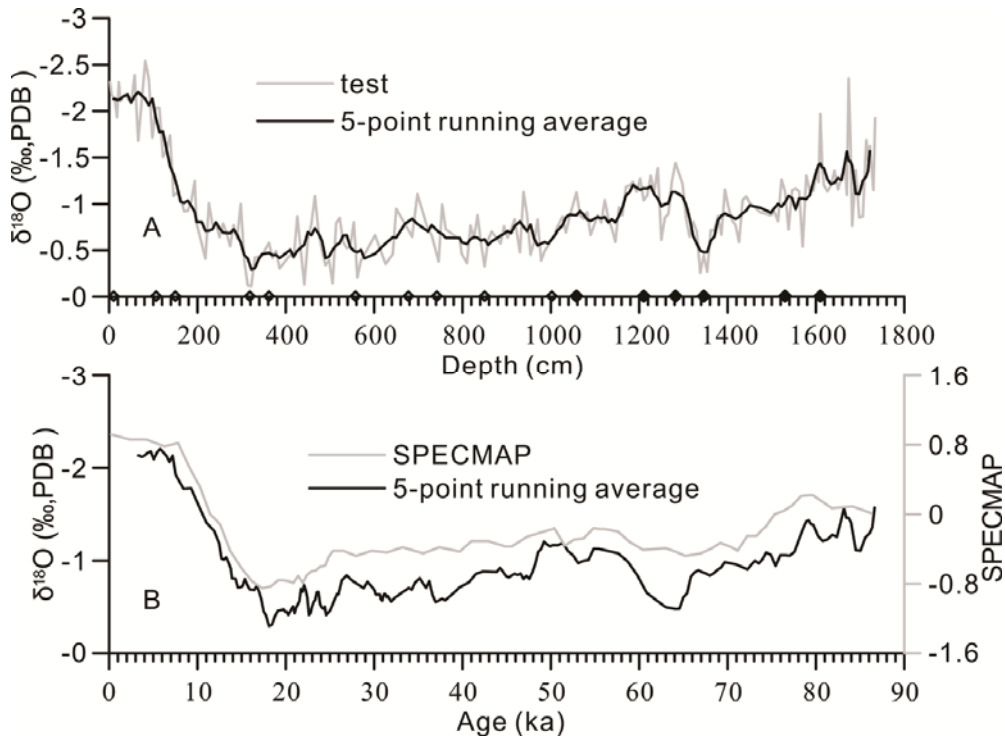
带格式的: 居中

Figure 1. The pink star indicates core CSH1. The open circles means other cores mentioned in this study and the triangles denote the stalagmite caves in East China. Arrows denote simplified surface currents in the study region. The blue dashed curve stands for the -120 m isobath.



带格式的：居中

Figure 2. Monthly temperature and salinity for the upper 400 m of the water column in the northern Okinawa Trough at 131-132°E and 28-29°N. (Data source: JODC Data On-line Service System, <http://www.jodc.go.jp/service.htm>).



1
2
3 Figure 3. (A) $\delta^{18}\text{O}$ of planktonic foraminifera *G.ruber* plotted against depth (cm) for core
4 CSH1. The age control point for AMS ^{14}C and $\delta^{18}\text{O}$ are indicated by the symbol \diamond and \blacklozenge ,
5 respectively. (B) Five-point running average $\delta^{18}\text{O}$ of planktonic foraminifera *G.ruber* for core
6 CSH1 and the SPECMAP (Martinson et al., 1987) plotted against age over the last 88 ka.

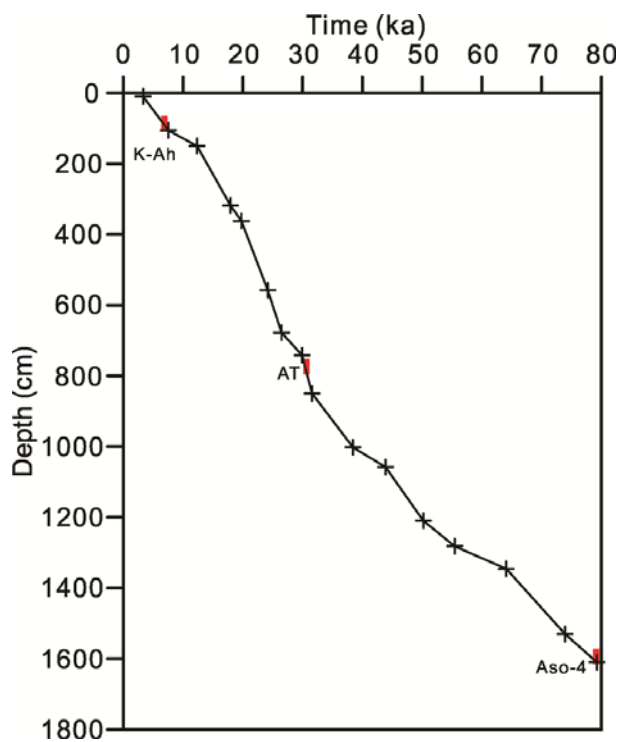
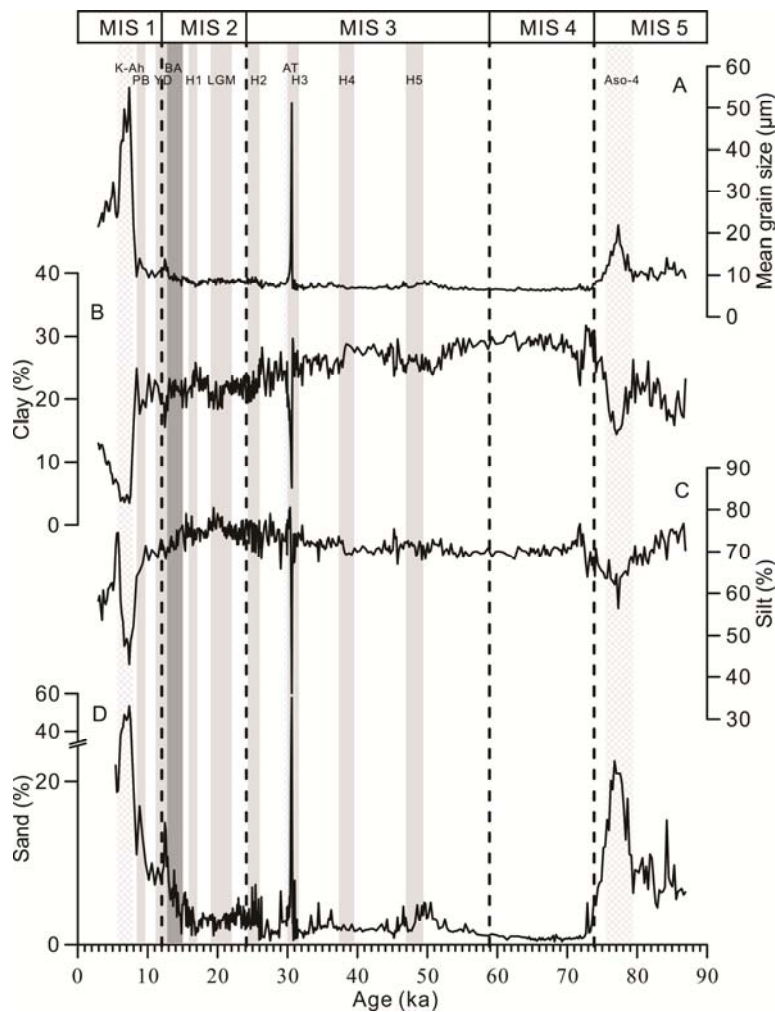
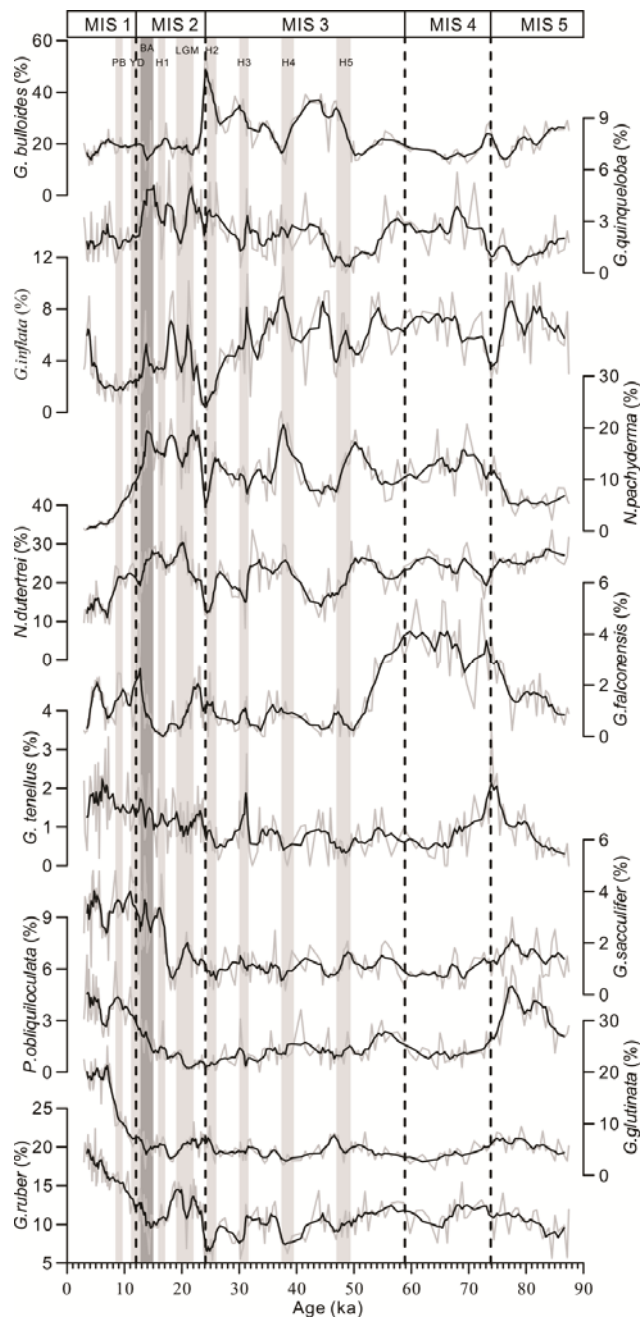


Figure 4. Plot of measured ages vs depth for core CSH1. Three known ash layers are indicated by red solid rectangles.



带格式的：居中

Figure 5. Time series plots for contents of sand, silt and clay and the mean grain size. Gray bars indicate the intervals of important climatic events. MIS 1, 2, 3, 4 and 5a represent marine isotope stages, respectively. K-Ah, AT, and Aso-4 refer to well known ash layers, widespread recorded in the Sea of Japan and the northern Okinawa Trough and indicated by the gray diagonal cross. PB, YD, BA, H1, H2, LGM, H3, H4, and H5 refer to Preboreal, Younger Dryas, Bolling/Allerod, Heinrich 1, Heinrich 2, Last Glacial Maximum, Heinrich 3, Heinrich 4 and Heinrich 5, respectively.



带格式的：居中

1
2
3 Figure 6. Time series plots for the abundance of dominant species of planktonic foraminifera
4 in core CSH1. Gray bars are the same as those in Fig. 5.

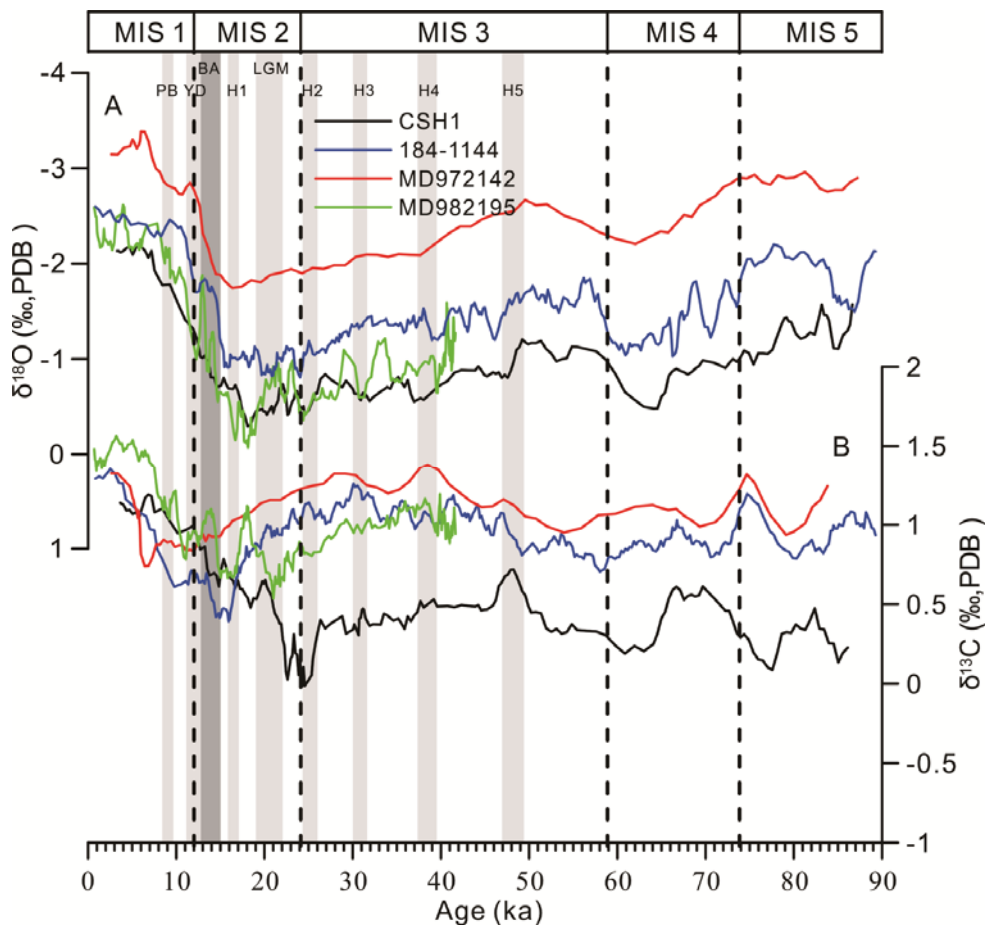


Figure 7. Time series plots of $\delta^{18}\text{O}$ and $\delta^{13}\text{C}$ of planktonic foraminifera and in contrast with the records in cores MD982195 (Ijiri et al., 2005), MD972142 (Chen et al., 2003) and site 184-1144 (Buhring, 2001). Gray bars are the same as those in Fig. 5.

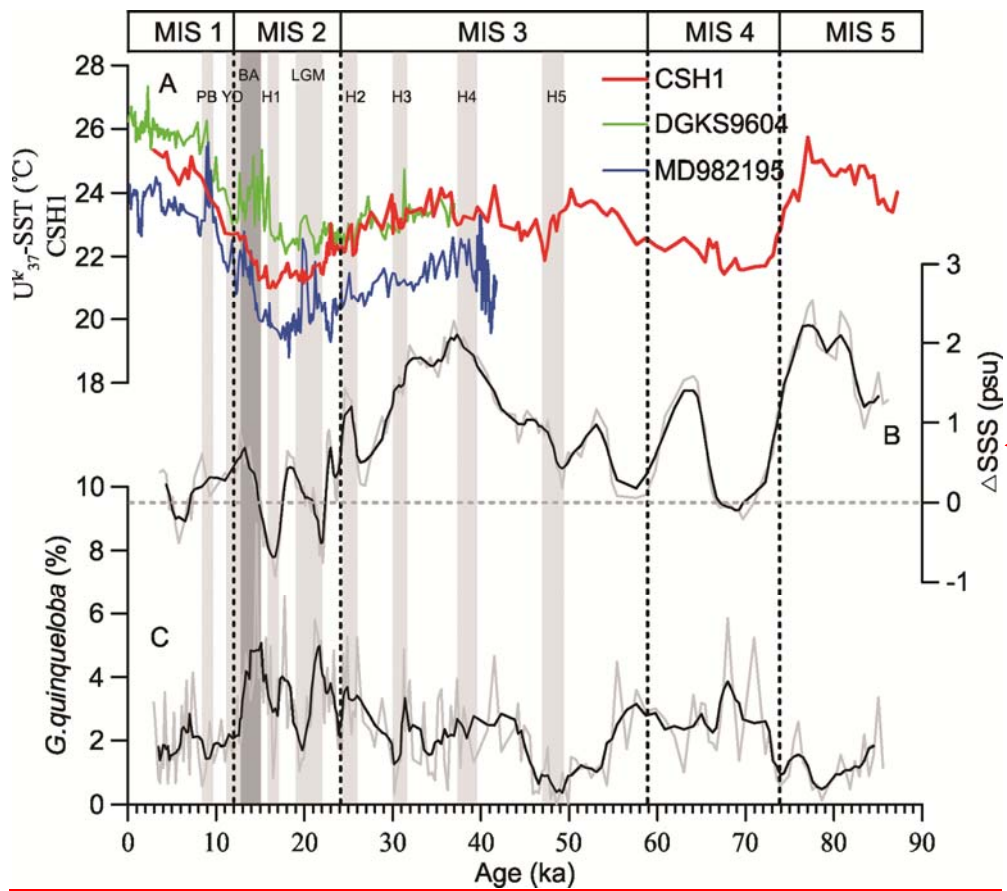
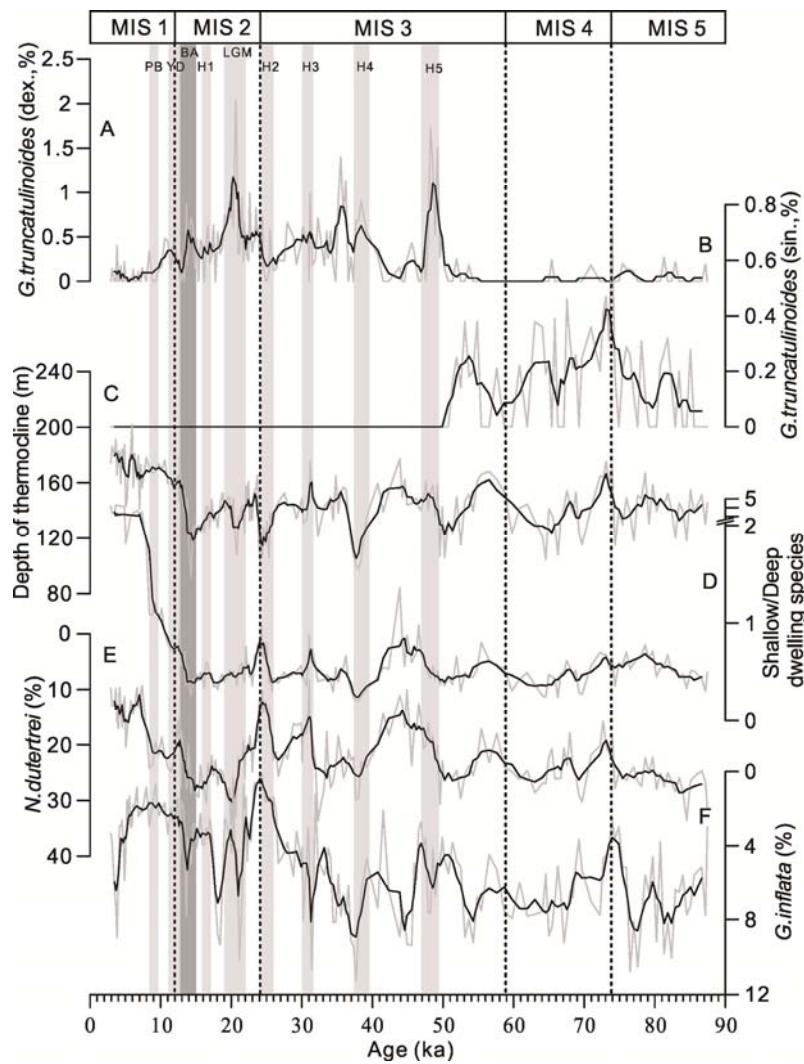


Figure 8. Time series plots of temperature and salinity in core CSH1 and compared to other records in cores MD982195 (Ijiri et al., 2005) and DGKS9604 (Yu et al., 2009). Gray bars are the same as those in Fig. 5. Salinity values are given as the difference from the present-day climate, ΔS .

带格式的：居中



带格式的：居中

Figure 9. Time series plots of abundance of *G.truncatulinooides*, depth of thermocline, the ratio of shallow/deep species, abundance of *N.dutertrei*. Both the distributions of *N.dutertrei* and *G.inflata* are related to DOT, but they show different down-core profiles in core CSH1. Gray bars are the same as those in Fig. 5.

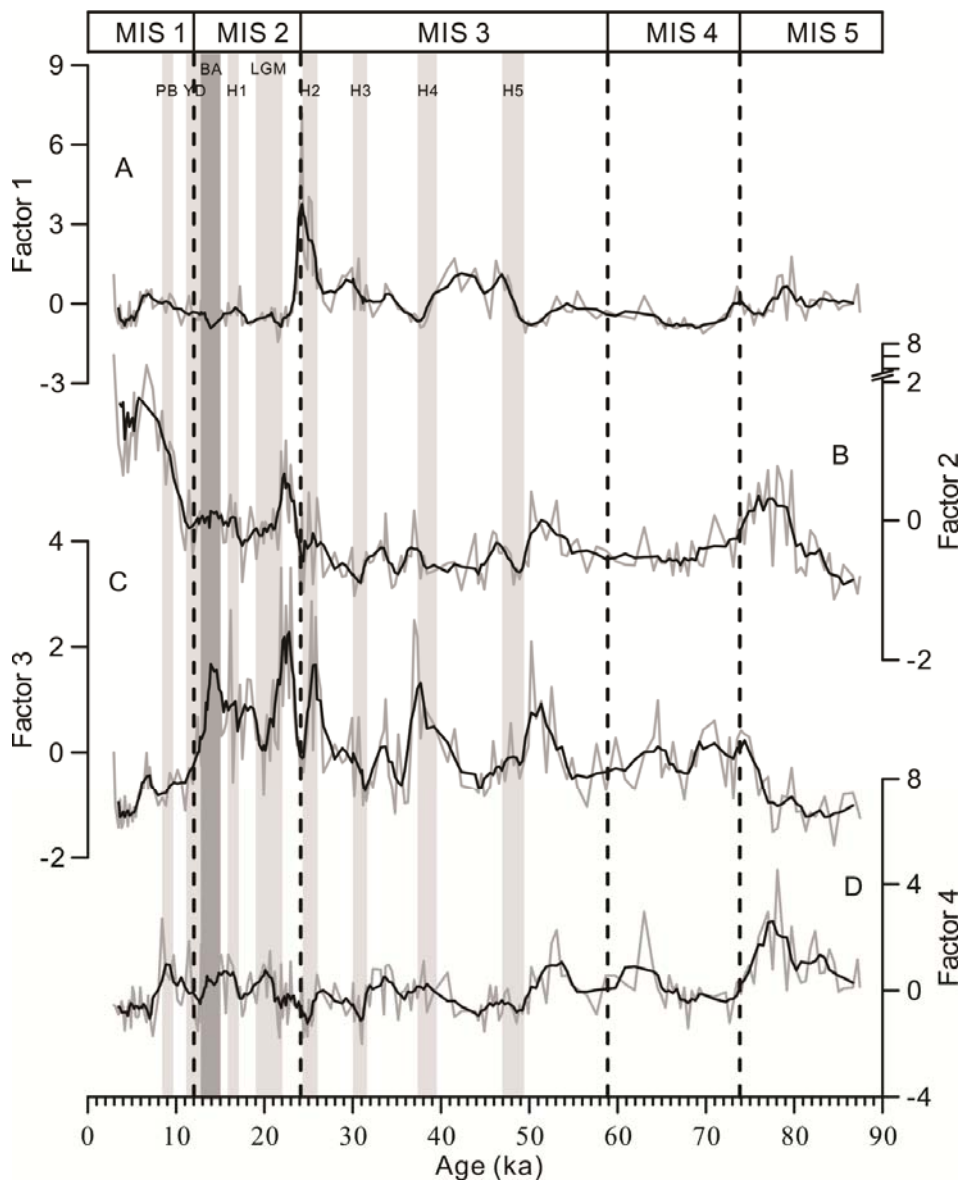


Figure 10. Time series plots of the four main factor scores for planktonic foraminiferal assemblages. Gray bars are the same as those in Fig. 5.

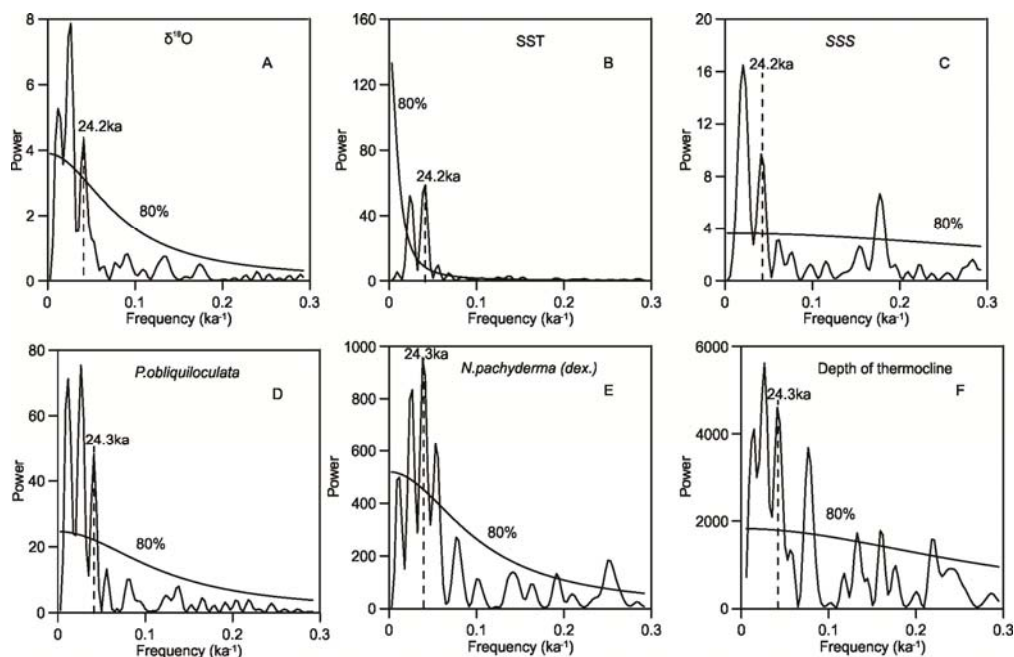


Figure 12. Power spectrum of the $\delta^{18}\text{O}$, SST, SSS, depth of thermocline, and the abundances of *P.obliquiloculata* and *N.pachyderma* (dex.) time series. All proxies show a common frequency at the precession cycles (near 24 ka).

带格式的: 字体: (中文) + 中文正文

带格式的: 字体: (中文) + 中文正文, 小四

带格式的: 字体: (默认) Times New Roman, (中文) + 中文正文, 小四, 上标

带格式的: 字体: (默认) Times New Roman, (中文) + 中文正文, 小四

带格式的: 字体: (默认) Times New Roman, (中文) + 中文正文, 小四, 倾斜

带格式的: 字体: (默认) Times New Roman, (中文) + 中文正文, 小四

带格式的: 字体: (默认) Times New Roman, (中文) + 中文正文, 小四, 倾斜

带格式的: 字体: (默认) Times New Roman, (中文) + 中文正文, 小四

带格式的: 字体: (中文) + 中文正文, 小四

带格式的: 字体: (中文) + 中文正文

带格式的: 字体: (中文) + 中文正文